Molecular Biology of the Cell
Vol. 19, 4942–4955, November 2008

In Vitro Budding of Intralumenal Vesicles into Late Endosomes Is Regulated by Alix and Tsg101

Thomas Falguières, Pierre-Philippe Luyet, Christin Bissig, Cameron C. Scott, Marie-Claire Velluz, and Jean Gruenberg

Biochemistry Department, University of Geneva, 1211 Geneva 4, Switzerland

Submitted March 5, 2008; Revised July 18, 2008; Accepted August 26, 2008
Monitoring Editor: Sandra L. Schmid

Endosomes along the degradation pathway leading to lysosomes accumulate membranes in their lumen and thus exhibit a characteristic multivesicular appearance. These lumenal membranes typically incorporate down-regulated EGF receptor destined for degradation, but the mechanisms that control their formation remain poorly characterized. Here, we describe a novel quantitative biochemical assay that reconstitutes the formation of lumenal vesicles within late endosomes in vitro. Vesicle budding into the endosome lumen was time-, temperature-, pH-, and energy-dependent and required cytosolic factors and endosome membrane components. Our light and electron microscopy analysis showed that the compartment supporting the budding process was accessible to endocytosed bulk tracers and EGF receptor. We also found that the EGF receptor became protected against trypsin in our assay, indicating that it was sorted into the intraendosomal vesicles that were formed in vitro. Our data show that the formation of intralumenal vesicles is ESCRT-dependent, because the process was inhibited by the K173Q dominant negative mutant of hVps4. Moreover, we find that the ESCRT-I subunit Tsg101 and its partner Alix control intralumenal vesicle formation, by acting as positive and negative regulators, respectively. We conclude that budding of the limiting membrane toward the late endosome lumen, which leads to the formation of intraendosomal vesicles, is controlled by the positive and negative functions of Tsg101 and Alix, respectively.

INTRODUCTION

In eukaryotic cells, molecules of the plasma membrane, ligands and solutes are internalized into early endosomes, from where they can be recycled back to the plasma membrane, transported to the *trans*-Golgi network, or targeted to late endosomes and lysosomes (Gruenberg, 2001; Maxfield and McGraw, 2004; Mayor and Pagano, 2007). The latter pathway is followed in particular by ubiquitinated signaling receptors that need to be down-regulated. These receptors are incorporated into invaginations of the early endosomal membrane that form within their lumen (Hurley and Emr, 2006), thus giving rise to nascent multivesicular bodies (MVBs) or endosomal carrier vesicles (ECVs; Gruenberg and Stenmark, 2004; Piper and Katzmann, 2007), which function as intermediates between early and late endosomes. Eventually, intralumenal vesicles are delivered to lysosomes, where they are degraded together with their receptor cargo.

Major progress has been made in our understanding of the molecular mechanisms that control the sorting of ubiquitinated receptors, in particular the epidermal growth factor (EGF) receptor (Hurley and Emr, 2006; Slagsvold *et al.*, 2006; Piper and Katzmann, 2007; Williams and Urbe, 2007). These receptors interact via the ubiquitin moiety with hepatocyte growth factor–regulated tyrosine kinase substrate (Hrs), which in turn binds clathrin and phosphatidyl-inositol-3-phosphate (PtdIns3P), thereby concentrating the receptor in early endosomal membrane domains (Raiborg *et al.*, 2001; Urbe *et al.*, 2003; Raiborg *et al.*, 2006). Hrs then recruits the tumor susceptibility gene 101 (Tsg101) subunit of ESCRT-I (endosomal sorting complex required for transport; Bache *et al.*, 2003a), initiating the sequence of events mediated by ESCRT-I, II, and III that eventually leads to receptor incorporation into intralumenal vesicles (Hurley and Emr, 2006; Slagsvold *et al.*, 2006; Williams and Urbe, 2007). Evidence shows that this PtdIns3P-, Hrs-, and ESCRT-based sorting mechanism is coupled to the membrane invagination process. The number of intralumenal vesicles within endosomes is decreased after PtdIns 3-kinase inhibition (Reaves *et al.*, 1996; Fernandez-Borja *et al.*, 1999; Futter *et al.*, 2001), and after Hrs knockout in *Drosophila melanogaster* (Lloyd *et al.*, 2002) or knockdown in mammalian cells (Bache *et al.*, 2003b; Razi and Futter, 2006). Presumably, Hrs, by initiating ESCRT recruitment, is indirectly responsible for intralumenal vesicle formation (Bache *et al.*, 2003a). In yeast, class E Vps (vacuolar protein sorting) mutants, including Vps27p/Hrs and ESCRTs, induce the formation of an aberrant endosome (Raymond *et al.*, 1992) that contains endocytosed membrane proteins (Babst, 2005). However, depletion of the ESCRT-I subunit Tsg101 in mammalian cells causes pleiotropic changes in early endosome morphology, including tubulation, reduction in the number of lumenal vesicles (Razi and Futter, 2006), and formation of a class E-like compartment (Doyotte *et al.*, 2005). Although there is no

This article was published online ahead of print in *MBC in Press* (http://www.molbiolcell.org/cgi/doi/10.1091/mbc.E08–03–0239) on September 3, 2008.

Address correspondence to: Jean Gruenberg (jean.gruenberg@biochem.unige.ch).

Abbreviations used: Alix, ALG-2 interacting protein X; DPX, *p*-xylène-bis-pyridinium bromide; EGF, epidermal growth factor; ESCRT, endosomal sorting complex required for transport; HPTS, 8-hydroxypyrene-1,3,6-trisulfonic acid; HRP, horseradish peroxidase; Hrs, hepatocyte growth factor–regulated tyrosine kinase substrate; LBPA, lysobisphosphatidic acid; PNS, postnuclear supernatant; PtdIns3P, phosphatidyl-inositol-3-phosphate; siRNA, small interfering RNA; Tsg101, tumor susceptibility gene 101.

doubt that Hrs and ESCRTs control lysosomal targeting of ubiquitinated proteins, the mechanism responsible for the membrane invagination process remains elusive.

In this study, we describe a novel biochemical approach that reconstitutes the formation of lumenal vesicles within late endosomes, so that the process could be investigated directly. The assay measures the entrapment of a small nonmembrane permeant dye into newly formed intralumenal vesicles. The formation of intralumenal vesicles was time-, temperature-, pH-, and energy-dependent and required both cytosolic factors and endosomal membrane components. By combining this assay with electron microscopy, we characterized the compartment that supports lumenal vesicle formation as late endosome accessible to both bulk tracers and EGF receptor. Conversely, the EGF receptor became protected against trypsin during the assay, indicating that it was sorted into newly formed lumenal vesicles. We found that lumenal vesicles, although bathed within acidic endosomes, remained neutral over the time course of the assay. Finally, we used this assay to investigate the possible roles of the ESCRT-I subunit Tsg101 and ALG-2–interacting protein X (Alix), a protein that interacts with Tsg101 (Strack *et al.*, 2003; von Schwedler *et al.*, 2003) and plays a role in endosome membrane dynamics (Abrami *et al.*, 2004; Matsuo *et al.*, 2004; Le Blanc *et al.*, 2005). We find that both Tsg101 and Alix play a direct role in controlling the formation of intralumenal vesicles and EGF receptor sorting, but that they act as positive and negative regulators of the budding process, respectively.

MATERIALS AND METHODS

Cells, Reagents, and Antibodies

Baby hamster kidney cells (BHK-21; Gruenberg *et al.*, 1989) and BHK-21 cells expressing human green fluorescent protein (GFP)-tagged EGF receptor were cultured as described (Petiot *et al.*, 2003). Reagents were obtained from the following sources: protein assay reagent and horseradish peroxidase (HRP)–conjugated secondary antibodies from Bio-Rad Laboratories (Hercules, CA); HPTS (8-hydroxypyrene-1,3,6-trisulfonic acid), DAPI, and Texas Red–coupled EGF from Molecular Probes (Eugene, OR); DPX (*p*-xylene-bis-pyridinium bromide) from Chemie Brunschwig (Basel, Switzerland); U18666A (3-β-[2-(diethylamino)ethoxy]androst-5-en-17-one) from Biomol Research Laboratories (Plymouth Meeting, PA); Lipofectamine 2000, Oligofectamine, TRIzol, SuperscriptTMRT, and TOPO vector from Invitrogen (Basel, Switzerland); oligonucleotides and small interfering RNA (siRNA) from Qiagen (Germantown, MD); doxycycline from Clontech (Saint-Germain-en-Laye, France); glutathione Sepharose 4B from Amersham Biosciences (Little Chalfont, United Kingdom); anti-Tsg101 mAb (clone 4A10) from Genetex (San Antonio, TX); anti-EGF receptor and anti-annexin A2 monoclonal antibodies (BD Biosciences, San Diego, CA); anti-GFP mAb (Roche Diagnostics, Basel, Switzerland); anti-Vps4 polyclonal antibody (Santa Cruz Biotechnology, Santa Cruz, CA); fluororescently labeled secondary antibodies from Jackson ImmunoResearch Laboratories (West Grove, PA). Anti-Hrs was kindly provided by Harald Stenmark (Oslo, Norway). Empty peGFP, WT peGFP-Vps4A and peGFP-Vps4A K173Q were kindly provided by Wesley Sundquist (University of Utah School of Medicine, Salt Lake City, UT). The mAb against Lamp1 (4A1) has been described (Aniento *et al.*, 1993a), as well as polyclonal antibodies against Rab7 (Kobayashi *et al.*, 1998) and Alix (Chatellard-Causse *et al.*, 2002). Other chemicals and reagents were obtained from Sigma (St. Louis, MO).

Manipulations of Cells In Vivo

When indicated, subconfluent BHK cells were transfected 24 h after seeding with 4 μg wild-type (WT) or mutant Vps4A cDNA using 10 μl Lipofectamine 2000 for one 10-cm dish according to the manufacturer's instructions (4 μg cDNA and 10 μl Lipofectamine 2000 for one 10-cm dish) and were further incubated for 16 h. GFP and Vps4-GFP expression were checked by confocal microscopy and Western blotting. In some experiments, we used BHK cells expressing the human EGF receptor tagged with the GFP under the control of a tetracycline promoter (Petiot *et al.*, 2003). Cells were mock-treated or treated with siRNAs against Alix, Tsg101, or both for 3 d. EGF receptor expression was induced with 1 μg/ml doxycycline 24 h before the experiment. Cells were serum-starved for 1 h at 37°C in the presence of 10 μg/ml cycloheximide (which was maintained throughout the experiment). Finally, EGF was bound to the plasma membrane by incubating cells with 200 ng/ml EGF for 1 h on ice. Then, cells were incubated for increasing time periods at 37°C. Postnuclear supernatants (PNSs) were prepared and used in our in vitro assay. The knockdown of Alix and Tsg101 was always controlled by Western blotting.

In RNA interference (RNAi) experiments, RNA from BHK cells was extracted with TRIzol according to the manufacturer's instructions. Then, 0.5 μg total RNA was used for reverse transcription with SuperscriptTMRT using random hexamers. The transcribed DNA was subjected to PCR using two primers (designed in highly conserved regions among several species) for each locus to be analyzed: Alix (forward primer: 5′-GGTGCAGCTGAAGAAGACCT-3′; reverse primer: 5′-CAGGTTCTGCTCTGCAAT-3′; Chevallier *et al.*, 2008), Tsg101 (forward primer: 5′-CCTCCTGTGACCACTGTTCCC-3′; reverse primer: 5′-GTGCCCTTAGCTGGAACTG-3′) and Hrs (forward primer: 5′-TGTACCTGATCCAGG CCTGGG-3′; reverse primer: 5′-GGTCGATGTCCTCAGCCAGAG-3′). Then specific PCR bands were excised and purified. The DNA was cloned into a TOPO vector according to the manufacturer's instructions. TOP10 bacteria were transformed and grown; DNA was isolated and further sequenced for analysis by Fasteris SA (Geneva, Switzerland). Sequences were aligned with Vector NTI AlignX software (Invitrogen); siRNAs were designed with the siRNA design tool (Qiagen) and blasted to ensure that sequences were unique: control siRNA (anti-VSVG), 5′-AAAAAGGAAACTGGAAAAATG-3′; Alix, 5′-AAGCCGCTGGTGAAGTTCATC-3′; Tsg101 no. 1, 5′-AACTGAGATGGCGGATGAAGG-3′; Tsg101 no. 2, 5′-AAGTTCTGCTCTGGAGAAAAT-3′, Tsg101 no. 3, 5′-AAGGGCCACCAGAAACTGGAA-3′; and Hrs, 5′-AAGGACATGTCTTCCCAGAAT-3′. In RNAi experiments, subconfluent BHK cells were incubated for 24 h after seeding with 0.1 μM (final concentration) 21-nucleotide RNA duplexes with 2-nucleotide 3′-(2-deoxy)-thymidine overhangs and Oligofectamine (volume ratio 1:1, following the manufacturer's instructions) and then were further incubated for 72 h (Le Blanc *et al.*, 2005).

Biochemical Assay Measuring Budding of Intralumenal Vesicles In Vitro

PNSs were typically prepared from one dish of BHK cells (≈15 mg/ml) per condition (Gruenberg *et al.*, 1989) and used in the in vitro invagination assay following protocol 1 (Figure 1A). The PNS (215 μl) was adjusted to a final volume of 300 μl with 1 mM HPTS, 100 mM KCl, 12.5 mM HEPES-NaOH, pH 7.4, 1.5 mM MgOAc, 1 mM DTT (final concentrations) in the presence of an ATP-regenerating or -depleting system (Gruenberg *et al.*, 1989). When indicated, the reaction mixture was supplemented with 1 μM bafilomycin A1 or 5 μM nigericin. This mix was incubated at 37°C for the indicated time period, the reaction was stopped on ice, and excess HPTS was quenched with 100 μl of 200 mM DPX in 20 mM HEPES-NaOH, pH 7.4, 150 mM NaCl. Then, early and late endosome fractions were prepared by flotation in a step sucrose gradient (Gorvel *et al.*, 1991; Aniento *et al.*, 1993a). In some experiments, we used in the assay PNS prepared from cells that had been incubated with 2 mg/ml HRP for 10 min at 37°C and then for 40 min without HRP to label late endosomes (Gruenberg *et al.*, 1989). At the end of the assay, the reaction mixture was centrifuged at 120,000 × *g*, and HRP was quantified in pellets and supernatants to determine endosome latency after in vitro incubation (Gruenberg *et al.*, 1989; Gu *et al.*, 1997). To measure EGF receptor incorporation in intralumenal vesicles in vitro, late endosomes from cells expressing GFP-EGF receptor were prepared on gradients 30 min after stimulation with EGF. The fractions were incubated for 15 min at 37°C with or without 250 μg TPCK (*N*-tosyl-L-phenylal-anine chloromethyl ketone)-treated trypsin (Sigma) per mg endosome protein. The reaction was stopped on ice by the addition of a fivefold molar excess of soybean trypsin inhibitor (Sigma). After 15 min, samples were processed for SDS-PAGE and Western blotting analysis. EGF receptor was quantified from the blots (always at the same exposure times) with the Image Quant software (Amersham Biosciences).

Alternatively in protocol 2 (Figure 1A), early and late endosomes were first prepared using the same gradient. Then, 165 μl of the endosomal fraction was incubated with 50 μl rat liver cytosol (Aniento *et al.*, 1993b) added to the assay before the reaction was stopped on ice, and excess HPTS was quenched with DPX, as above. In some experiments, we used cytosols (20 mg/ml) from mock- or Tsg101 siRNA-treated BHK cells that had been prepared as described (Gu *et al.*, 1997). With either protocol, HPTS trapped in endosomes was measured by fluorescence (λ_{exc}: 413 nm/λ_{em}: 510 nm) as described (Matsuo *et al.*, 2004), and values were normalized to the protein content of the fractions. To measure the pH of intralumenal vesicles, HPTS fluorescence (λ_{em} = 510 nm) was also measured after excitation at the pH-sensitive wavelengths λ_{exc} = 397 and 445 nm (Willoughby *et al.*, 1998). For the standards, the fluorescence of 2 μM HPTS was measured at these wavelengths in 200 μl salt solution (150 mM NaCl) buffered between pH 5.4 and 10.4 with 20 mM MES (pH 5.4–6.6), HEPES (pH 6.8–8.2), and AMPSO (pH 8.4–10.4). Using these values, we established the exponential calibration curve $y = 5.10^{-7}e^{1.95x}$ with x = pH and y = fluorescence ratio at λ_{exc} = 397 and 445 nm, which was used to calculate pH values from the ratio of HPTS fluorescence. The same protocol was used to measure the lumenal pH of endosomes, after 60-min continuous HPTS internalization followed by preparation of early and late endosome fractions, as above. In all cases, the fractionation of endosomes was routinely monitored using Rab5 and both Rab7 and LBPA as early and late endosomal markers, respectively (Kobayashi *et al.*, 1998).

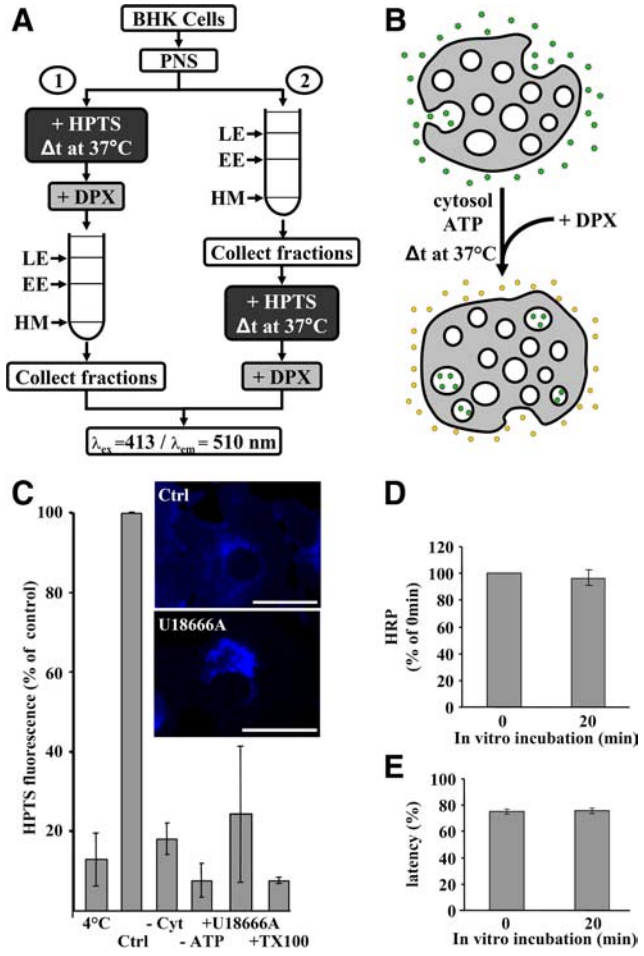

Figure 1. In vitro assay measuring HPTS incorporation. (A) Schematic representation of the assay. Membranes were incubated with HPTS before (protocol 1) or after (protocol 2) endosome fractionation, using PNS (protocol 1) or isolated late endosome fractions (protocol 2). EE, early endosomes; LE, late endosomes; HM, heavy membranes. HPTS incorporated into late endosomes is measured by fluorescence at the indicated wavelengths. (B) After incubation at 37°C in the presence of cytosol and ATP, HPTS (green stars) becomes protected from DPX, whereas extraendosomal HPTS is quenched by DPX (yellow symbols). (C) The in vitro assay was performed with protocol 2 at 4 or 37°C for 20 min (Ctrl, control), without cytosol (−Cyt), or without ATP (−ATP). Alternatively, cells were pretreated with 3 μg/ml U18666A for 16 h at 37°C before the experiment (+U18666A). +TX-100 indicates that late endosome fractions were solubilized with 1% Triton X-100. For each condition, the means (± SEM) of at least three independent experiments are shown. Inset, the distribution of cholesterol in control and U18666A-treated cells, revealed after filipin staining by fluorescence microscopy. Bars, 20 μm. (D) BHK cells were incubated with HRP for 10 min at 37°C followed by a 40-min chase without the marker to label late endosomes. PNSs were prepared and incubated for the indicated time at 37°C using protocol 1. Late endosome fractions were collected and centrifuged at high speed, and HRP was quantified in supernatants and pellets. The total HRP content of late endosome pellets after the assay is expressed as a percentage of the amounts initially present. Means (± SEM) of three independent experiments are represented. (E) The distribution of HRP in high-speed supernatants and pellets from D was used to calculate the latency (as the percentage of membrane-enclosed HRP). Means (± SEM) of three independent experiments are represented.

Immunofluorescence and Quantification Methods

We used BSA coupled to Cy3 (BSA-Cy3; Amersham Biosciences) to label endosomes with a fluid phase tracer. Cells were incubated with 0.1 mg/ml BSA-Cy3 for 90 min at 37°C and analyzed by immunofluorescence (Gu *et al.*, 1997; Kobayashi *et al.*, 1998). Samples were viewed with a LSM 510 Meta confocal microscope from Zeiss (Feldbach, Switzerland), using the same laser power and acquisition settings for each condition in parallel experiments. Picture analysis, quantification and processing were carried out with the LSM software (Zeiss) and Photoshop 7.0 (Adobe, San Jose, CA). When indicated, PNS was prepared from BSA-Cy3–labeled cells and used in the in vitro assay measuring intraendosome vesicle budding (protocol 1). Then, endosomal fractions recovered from the gradient were used to quantify HPTS present in intralumenal vesicles and BSA-Cy3 (λ_{exc} = 545 nm/λ_{em} = 570 nm). Alternatively, endosomes were mounted between glass slides and coverslips without any chemical or physical fixation, and observed directly by confocal microscopy. Then quantification was done with the ImageJ software (http://rsb.info.nih.gov/ij/; NIH, Bethesda, MD). We counted 200 HPTS-positive structures as BSA-Cy3 positive or negative from four different pictures, and results were expressed as the percentage of HPTS-positive structures that colocalized with BSA-Cy3.

To follow the traffic of the EGF receptor, BHK cells stably expressing human EGF receptor-GFP were treated or not for 24 h with 1 μg/ml doxycycline and then were serum-starved for 1 h at 37°C. Cells were then incubated on ice sequentially with the mAb against the EGF receptor for 20 min followed by Cy5-coupled secondary antibody for 20 min and 200 ng/ml Texas Red-EGF for 1 h and were rinsed in the cold with PBS between incubations. Finally, cells were incubated for 50 min at 37°C and processed for indirect immunofluorescence as above.

To monitor the back-fusion process with the endosome limiting membrane, lumenal vesicles were first preloaded with HPTS after incubating the PNS with HPTS for 20 min at 37°C (protocol 1). Then, late endosomes were prepared by fractionation and mixed on ice as described in protocol 2 for HPTS incorporation with or without 20 mM DPX, except that HPTS was omitted. To measure HPTS release from endosomes, aliquots of the mixture were mounted between slides and coverslip and analyzed by confocal microscopy, as above. In three independent experiments, micrographs of 25 HPTS-positive structures were captured every 8 s and analyzed and quantified over a 10-min period with the ImageJ software.

Electron Microscopy and Quantification

To visualize the formation of intralumenal vesicles, PNS was prepared and used in the in vitro assay (protocol 1) with 1 μM HPTS and nonreactive nanogold particles ($OD_{520\ nm}$ = 1.0; Nanoprobes, Yaphank, NY). Endosomes were then recovered and HPTS was quantified by fluorometry (see above). Aliquots were concentrated by ultracentrifugation at 55,000 rpm for 30 min in a TLS55 rotor (TL100 ultracentrifuge; Beckman Coulter, Fullerton, CA). Pellets were carefully recovered in 50 μl of 2% glutaraldehyde in PBS, incubated for 10 min at room temperature, and mixed with an equal volume of 4% low-melting agarose type VII (preheated at 37°C). Then, the agarose was solidified on ice, and agarose blocks were cut in small pieces and successively washed with PBS, 50 mM NH_4Cl in PBS, PBS containing 1% BSA, and water. Gold enhancement (Nanoprobes) was performed for 5 min at room temperature, according to manufacturer's instructions, and after washes, samples were processed for electron microscopy (Parton *et al.*, 1992). After this long enhancement treatment, gold particles showed a heterogeneous size distribution, presumably because of variability in gold particle accessibility to the enhancer. In some experiments, the endosome lumen was prelabeled in vivo after continuous endocytosis for 90 min at 37°C of 15-nm BSA-gold (Aurion, Wageningen, Netherlands) at $OD_{520\ nm}$ = 10 in medium containing 1% BSA. Cells were then used as above in the in vitro assay using nanogold. Then, gold enhancement was for only 1 min at room temperature so that the diameter of enhanced nanogold particles remained <10 nm. Alternatively, endosomes were prelabeled in vivo with anti-EGF receptor gold particles. Cells expressing the EGF receptor were serum-starved and incubated on ice with monoclonal antibodies against the receptor (as in the light microscopy experiments above), and 200 μg/ml EGF and 15-nm protein A-gold (Cell Microscopy Center, Utrecht, The Netherlands). The complex was endocytosed for 50 min at 37°C, PNS was prepared and used in the in vitro assay with nanogold (gold enhancement was for 1 min, as above). For quantification, we counted the number of gold particles per profile (inside or outside) in 90 different profiles from three independent experiments for each siRNA condition, and 60 different profiles from two independent experiments for EGF receptor labeling, respectively. Then, results were expressed as averages of numbers of gold particles per isolated structure. The perimeter of isolated late endosomal structures after siRNA was determined for 20 isolated structures from three independent experiments using the NIH ImageJ software.

Other Methods

The fluorescence analysis of cholesterol distribution after filipin staining was performed as described (Kobayashi *et al.*, 1999). Recombinant Alix, Alix-GST and Annexin A2 were prepared and purified as described (Chatellard-Causse *et al.*, 2002; Matsuo *et al.*, 2004; Morel and Gruenberg, 2007), as was Alix-GST pulldown from rat liver cytosol (Cavalli *et al.*, 2001). When needed, cells were treated with 3 μg/ml U18666A during 16 h (Mayran *et al.*, 2003). Protein quantification (Bradford, 1976) and SDS-PAGE (Laemmli, 1970) were de-

scribed, as was Western blotting (Burnette, 1981). Blot exposure times were always within the linear range of detection, and signal intensities were quantified using the ImageQuant software (Molecular Dynamics, Sunnyvale, CA).

RESULTS

In Vitro Reconstitution of Intraendosomal Budding

We designed a novel biochemical assay to investigate the mechanisms that control the formation of intralumenal vesicles within late endosomes. These were prepared by flotation in sucrose step gradients, using a well-established fractionation protocol, and recovered at their characteristic low buoyancy (Gorvel *et al.*, 1991; Aniento *et al.*, 1993a; Kobayashi *et al.*, 1998). Then, the purified late endosomes were incubated in vitro with cytosol, ATP, and the small, water-soluble and nonmembrane-permeant fluorescent dye HPTS (Figure 1A, protocol 2). If new vesicles formed by inward budding from the limiting membrane during the in vitro incubation, they would trap HPTS in their lumen, which is topologically equivalent to, but not continuous with, the extraendosomal environment. Then, the excess dye present in the solution was quenched with the nontoxic and nonmembrane permeant reagent DPX (Tedesco and Matile, 1999; Matsuo *et al.*, 2004; Supplemental Figure S1A). Finally, the DPX-protected fluorescence emitted by HPTS present within newly formed intraendosomal vesicles was quantified (Figure 1B). Under these conditions, the specific HPTS signal was approximately twice the background (Supplemental Figure S1C), because excess HPTS remained present in the mixture (Figure 1A).

We first determined whether endosomes remained intact under our conditions of in vitro incubation. To this end, we used PNSs prepared from cells that had internalized HRP for 10 min at 37°C followed by a 40-min chase without the marker to label late endosomes (Gruenberg *et al.*, 1989). The amounts of endosome-associated HRP (Figure 1D) and the latency of HRP (Figure 1E) were not affected by the in vitro incubation, demonstrating that endosome rupture did not occur in the assay. The HPTS incorporation process was selective, because it required the presence of cytosol, and was inhibited in the cold or without ATP (Figure 1C). In addition, the dye became membrane-enclosed during the assay, because HPTS fluorescence was fully quenched by DPX after permeabilization with Triton X-100 (Figure 1C). To further demonstrate that HPTS had been properly incorporated within endosomal organelles, PNSs were first incubated with HPTS. After DPX quenching, late endosomes were prepared by flotation using the same gradient (Figure 1A, protocol 1), and their HPTS content was measured. With this protocol, the specific HPTS signal was ~10-fold higher than the background (Supplemental Figure S1B) because excess HPTS was removed during fractionation (Figure 1A). Using this alternative assay, HPTS incorporation exhibited the same temperature, cytosol, and energy dependence as with protocol 2 in Figure 1A (data not shown). Protocol 1 was used thereafter, unless otherwise indicated. Early endosomes also supported HPTS incorporation with either protocol (see Figures 5B and 6B, and Supplemental Figure S6D), as expected because the invagination process begins in early endosomes (Gruenberg and Stenmark, 2004; Piper and Katzmann, 2007). By contrast, a heavy membrane fraction recovered from the same gradient (see Figure 1A), which contained the plasma membrane and early biosynthetic membranes but not endosomes (Gu *et al.*, 1997; Harder *et al.*, 1997; Rojo *et al.*, 1997), did not support HPTS incorporation with either protocol (data not shown). These observations demonstrate that HPTS was incorporated from the solution into membrane organelles, presumably late endosomes, and that this process required energy and depended on cytosolic factors.

Endosomes Support the In Vitro Invagination Process

To further characterize the compartments that supported HPTS incorporation in vitro, BHK cells were incubated with BSA-Cy3 for 90 min at 37°C so that the fluid-phase tracer partially overlapped with the late endocytic marker Lamp1 (Figure 2A). After incubation with HPTS, freshly isolated late endosome fractions were analyzed by confocal microscopy without any fixation. HPTS accumulated within endosomes containing BSA-Cy3 (Figure 2B, arrowheads; Cy3 and HPTS fluorescence is shown in inverted contrast) in a time-dependent manner (Supplemental Figure S2, arrowheads). We then quantified HPTS accumulation biochemically by measuring the fluorescence emission of both HPTS and Cy3 in a fluorometer. Whereas BSA-Cy3 fluorescence remained constant in time as expected, HPTS emission increased over the time course of the experiments (Supplemental Figure S2; quantification in Figure 2C), as did the fluorescence intensity measured from confocal pictures (Figure 2D, the HPTS over Cy3 ratio is shown). Consistently, 81.33 ± 5.51% HPTS-labeled structures observed in the microscope after 10 min in vitro (Figure 2B) colocalized with internalized BSA-Cy3 (Figure 2E).

To further characterize the compartment supporting intralumenal vesicle formation, we made use of the drug U18666A, which mimics the cholesterol storage disorder Niemann-Pick type C and causes cholesterol accumulation in late endocytic compartments (Liscum and Faust, 1989; Simons and Gruenberg, 2000; Sturley *et al.*, 2004; Maxfield and Tabas, 2005). Treatment with U18666A did not interfere with endosome fractionation in protocols 1 and 2 (Figure 1A) under our experimental conditions (Mayran *et al.*, 2003). Strikingly however, drug treatment essentially abolished HPTS incorporation (Figure 1C). These data are consistent with previous observations that cholesterol accumulation interferes with late endosomal membrane dynamics, presumably because of altered membrane biophysical properties and reduced bilayer fluidity (Kobayashi *et al.*, 1999; Lebrand *et al.*, 2002; Sobo *et al.*, 2007b). Altogether, our observations demonstrate that intraendosomal vesicles have the capacity to bud from the limiting membrane of late endosomes, that the process can be reconstituted in vitro, and that it depends on both cytosolic factors and the dynamic properties of late endosome membranes.

Ultrastructural Analysis of Invagination-Competent Endosomes

As a next step, we used electron microscopy to visualize the formation of intralumenal vesicles within late endosomes. Cells were incubated with BSA-gold (15 nm) for 90 min at 37°C, and then the assay was carried out with HPTS together with nonreactive nanogold particles (1.5 nm), as an electron-dense tracer. Gold enhancement was then used to increase the size of these particles in the electron microscope analysis. We used this small gold size because larger gold particles (4 nm) were not efficiently incorporated into newly formed vesicles (Le Blanc *et al.*, 2005), possibly because their diameter was larger than the invagination neck. When the in vitro reaction was carried out at 4°C, the smaller nanogold particles were only rarely observed in endosomes (Figure 3A, arrows), presumably within invaginations of the limiting membrane (Matsuo *et al.*, 2004). By contrast, when the in vitro reaction was performed for 20 min at 37°C, nanogold particles accumulated in purified endosomes that contained endocytosed

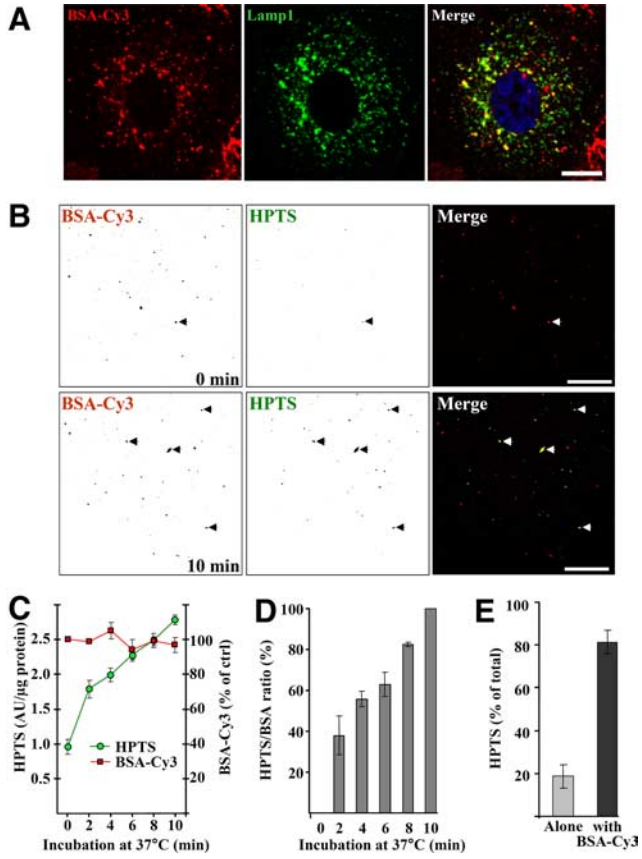

Figure 2. Endosomes preloaded with BSA-Cy3 incorporate HPTS. (A) After incubation with 0.1 mg/ml BSA-Cy3 for 90 min at 37°C (red, left panel), BHK cells were processed for confocal microscopy using antibodies against Lamp1 (green, middle panel). The right panel shows the merge of both channels. Nuclei were labeled with DAPI (blue, right panel). Bar, 10 μm. (B) After BSA-Cy3 internalization, PNSs of BHK cells were prepared and used in the in vitro assay with protocol 1 (Figure 1A) for 0–10 min at 37°C (other time points are shown in Supplemental Figure S2). Then, isolated late endosome fractions were analyzed by confocal microscopy. The micrographs showing BSA-Cy3 (red, left panels) and HPTS (green, middle panels) were inverted so that individual endosomes are easier to see. The right panels show the merged images in original colors. Arrowheads point at examples of structures positive for both HPTS and BSA-Cy3. Bars, 20 μm. (C) The experiment was as in B but the fluorescence of BSA-Cy3 and HPTS was quantified biochemically with a fluorometer. (D) Fluorescence signals were quantified for both channels and each time from the micrographs in B and Supplemental Figure S2. After background subtraction (i.e., 0-min time point), the HPTS over Cy3 fluorescence ratio is expressed as a percentage of the maximum value after 10 min. (E) From the experiments in B and Supplemental Figure S2, HPTS-positive structures were scored as BSA-Cy3 positive (■) or not (▨). (A and B) Representatives of three independent experiments. (C–E) Means (± SEM) of three independent experiments are represented.

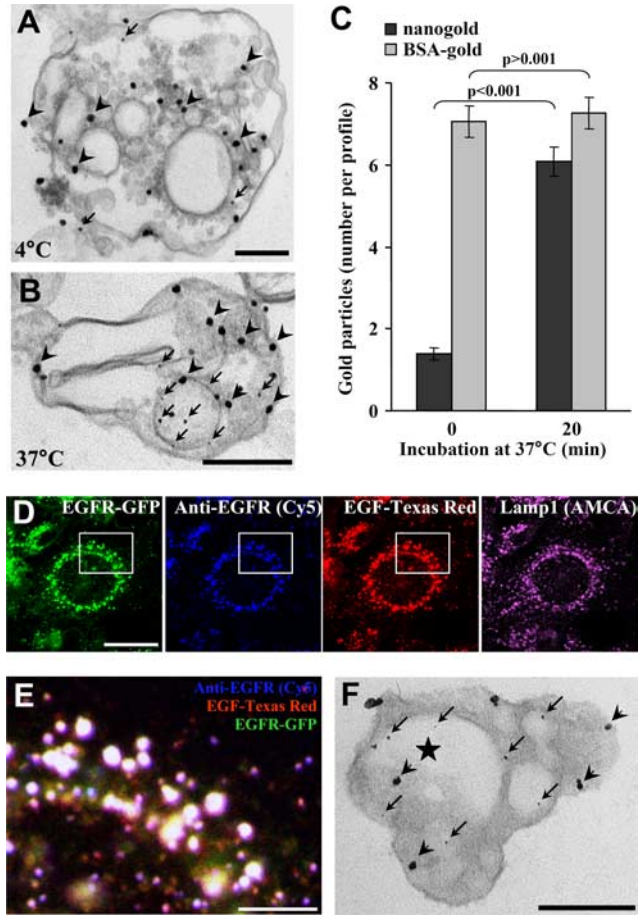

Figure 3. Ultrastructural analysis. (A and B) After BSA-gold (15 nm) internalization, the in vitro assay was performed with protocol 1 (Figure 1A), except that nanogold (1.3 nm) was coincubated with HPTS for 20 min at 4°C (A) or 37°C (B). Then, isolated late endosome fractions were processed for nanogold enhancement and electron microscopy. Arrowheads and arrows point at BSA-gold and enhanced nanogold particles, respectively. Bars, 200 nm. (A and B) Representatives of three independent experiments. (C) Quantification of the number of enhanced nanogold (■) and BSA-gold (▨) per profile in A and B. The chi-square test shows that the differences in the number of nanogold particles are significant ($p < 0.001$), whereas those in the number of BSA-gold particles are not ($p > 0.001$). Means (± SEM) of three independent experiments are shown. (D) Confocal analysis of doxycycline-treated BHK cells expressing a GFP-tagged human EGF receptor (green) under the control of a tetracycline promoter. After serum starvation, cells were subsequently incubated on ice with anti-EGF receptor antibody followed by Cy5-coupled anti-mouse antibody (blue) and Texas Red-coupled EGF (red). Then cells were shifted for 50 min at 37°C, fixed, and processed for indirect immunofluorescence against Lamp1, using an AMCA-coupled secondary antibody (purple). Bar, 20 μm. (E) The white box in D was magnified and shows the merge of the indicated markers. Bar, 5 μm. (F) After induction as in D, the EGF receptor was labeled on the cell surface with anti-EGF receptor antibody followed by protein A-gold (15 nm), and the complex was endocytosed for 50 min at 37°C. The assay was as in A–C with protocol 1 (Figure 1A), and samples were processed for electron microscopy. Arrowheads and arrows point at examples of protein A-gold–labeled EGF receptor and nanogold, respectively. The star indicates an internal vesicle containing both labeled EGF receptor and nanogold. Bars: 200 nm.

BSA-gold and exhibited the characteristic multivesicular morphology of late endosomes in BHK cells (Aniento *et al.*, 1993a; Kobayashi *et al.*, 1998; Figure 3B). Although the large endocytosed gold particles (Figure 3B, arrowheads) labeled the endosome lumen as expected, the small nanogold particles were observed in intraendosomal vesicles (Figure 3B, arrows), which closely resembled intralumenal vesicles observed in vivo (Le Blanc *et al.*, 2005). Quantification shows that the number of nanogold particles per late endosome (identified as containing BSA-gold) increased from 1.39 ± 0.16 to 6.09 ± 0.35 after incubation at 37°C, whereas the number of BSA-gold particles did not change significantly (7.07 ± 0.38 vs. 7.26 ± 0.38; Figure 3C).

Because it has been proposed that the endocytic transport of EGF receptor involves a subset of multivesicular endosomes (White *et al.,* 2006), we investigated whether the endocytosed receptor distributed within endosomes that support the formation of intralumenal vesicles in vitro. We used a BHK cell line expressing human EGF receptor tagged with GFP under the control of a tetracycline promoter (Petiot *et al.,* 2003; Supplemental Figure S3, A and B; the antibody we used only recognized the human receptor), because fractionation of endosomes is optimal in these cells with our protocol. After incubation on ice with anti-EGF receptor antibody followed by a Cy5-coupled secondary antibody, cells were challenged with 200 ng/ml Texas Red-human EGF and further incubated for 50 min at 37°C. The exoplasmic antibody and the GFP-tagged receptor colocalized with EGF in late endocytic compartments containing Lamp1 (Figure 3, D and E; low magnification views in Supplemental Figure S3).

We then used the same protocol for EGF stimulation and EGF receptor labeling, except that 15-nm protein A-gold replaced the secondary antibodies. The in vitro assay was carried out using nanogold as an electron-dense tracer for 20 min at 37°C as in Figure 3, A and B. Nanogold (Figure 3F, arrows) clearly accumulated within endosomes containing the EGF receptor (Figure 3F, arrowheads) when the reaction was carried out at 37°C, but not at 4°C as expected (Figure 3, A and B). In some micrographs, nanogold seemed to be present in the lumen of vesicles that also contained the EGF receptor (Figure 3F, star) perhaps suggesting that some nanogold and EGF receptor were incorporated together or that vesicles containing each marker underwent fusion within endosomes. Strikingly, we found that all labeled structures that we observed were positive for both gold sizes, nanogold and 15-nm anti-receptor gold particles, demonstrating that all endosomes containing the EGF receptor are invagination-competent in vitro and vice-versa.

Back-Fusion of Lumenal Vesicles with the Limiting Membrane of Late Endosomes

Because HPTS incorporation increased over the time course of our experiments (Figure 2, C and D), we investigated whether the dye continued to accumulate after longer times. HPTS incorporation leveled off after 15–20 min with either protocol (Supplemental Figure S4, A and B, protocols 1 and 2), eventually reaching a plateau with an apparent $t_{1/2} \approx 7.5$ min. It is thus possible that some factor required for the process became inactivated during the in vitro incubation. However, preincubation of both cytosol and endosomes for 20 min at 37°C (outline in Supplemental Figure S5A) did not significantly affect their competence to support HPTS incorporation in vitro during a second round of incubation (Supplemental Figure S5B), indicating that the assay did not rundown over this time course. Alternatively, it is possible that HPTS loaded into lumenal vesicles was being released into the solution via concomitant back-fusion of lumenal vesicles with the limiting membrane (van der Goot and Gruenberg, 2006). To test this possibility, PNSs were incubated with HPTS (Figure 1A, protocol 1) to preload endosomes during this first round of incubation. Then, endosomes were separated on gradients to remove excess HPTS and reincubated in vitro under the same conditions as used for protocol 2 (Figure 1A), except that HPTS was omitted. When analyzed in the confocal microscope, the number of HPTS-positive structures decreased over time (Figure 4B) to ≈20% of the initial fluorescence in 10 min (Figure 4D), and the process was ATP-dependent (Figure 4A, quantification in Figure 4C). These experiments indicate that HPTS can be released from endosomes into the medium via the fusion of lumenal vesicles with the late endosome limiting membrane.

Volume and pH of Intralumenal Vesicles

HPTS is a small solute that does not interact with membranes (Tedesco and Matile, 1999; Matsuo *et al.,* 2004). Thus, the volume of fluid entrapped within endosomes during vesicle formation could be estimated from the amounts of HPTS taken up and its concentration in the medium. After a 20-min incubation, when the plateau was reached (Supplemental Figure S4), 2AU HPTS were incorporated within endosomes per microgram endosomal protein, a value corresponding to 0.4 pmol HPTS/μg protein from the HPTS standard curve established with known concentrations. Because HPTS was present at a concentration of 1 mM in the reaction mixture, the volume of newly formed lumenal vesicles containing HPTS can be estimated to ≈0.4nl/μg endosomal protein. In a typical experiment, we used 24 μg endosome protein obtained with a yield ≈20% over the total homogenate from 2.5×10^7 cells (Gruenberg *et al.,* 1989; Aniento *et al.,* 1993a). We can thus estimate the lumenal volume to approximately 48 nl for 2.5×10^7 cells (i.e., 0.4 nl/μg $\times$ 24 μg $\times$ 100/20 = 48 nl) or ≈2 fl per cell. An analysis by electron microscopy using cytochemical and stereological methods showed that the total volume of late endosomes and lysosomes in BHK cells is ≈ 36.8 ± 11 fl, of which approximately half may represent endosomes (Griffiths *et al.,* 1989). The volume accessible to HPTS can thus be estimated to ≈ 10% of the endosome volume (i.e., 2 fl/18.4 fl $\times$ 100), a value that fits nicely with the late endosome ultrastructure (see *Discussion*).

One of the major characteristics of late endosomes is the low acidic pH (≈5.5) of their lumen (Mellman *et al.,* 1986; Forgac, 2007), but the pH of lumenal vesicles is not known—and may depend on the proton permeability of their membrane. HPTS fluorescence (λ_{em} = 510 nm) is pH-independent at λ_{exc} = 413 nm (Figure 5A). However, it decreases at λ_{exc} = 397 nm and increases at λ_{exc} = 445 nm, when the pH value is raised (Willoughby *et al.,* 1998; Figure 5A), and the ratio at these wavelengths (y) can be fitted into the exponential $y = 5.10^{-7}e^{1.95x}$, with x = pH, between pH 5.4 and 7.6 (Figure 5B). After the assay, early and late endosome fractions were collected and the pH of intralumenal vesicles was calculated in each fraction as 7.01 ± 0.11 and 7.16 ± 0.09, respectively (see the table in Figure 5B). In parallel but independent experiments, HPTS was endocytosed for 60 min at 37°C in vivo to label the endosomal content. After purification on gradient, we could estimate the lumenal pH of early and late endosomes as 6.06 ± 0.13 and 5.41 ± 0.14, respectively (see the table in Figure 5B), in very good agreement with the known pH of these compartments (Mellman *et al.,* 1986). These data further demonstrate that early and late endosomes are efficiently separated in the gradient. They also show that lumenal vesicles remain intact within endosomes during the assay, hence that HPTS indeed measures lumenal vesicle formation. It is possible that the pH of lumenal vesicles was neutralized by the buffer (12.5 mM HEPES) uptake from the medium. However, the maintenance of a steady cytosolic pH range is of paramount importance. Cells use pH regulatory mechanisms and powerful cellular buffers to maintain this pH range (Frelin *et al.,* 1988), thus the pH of newly formed lumenal vesicles may equally well be neutralized in vivo.

Next, we tested whether late endosomes remained acidic during incubation in the in vitro assay. When late endosomes that had been labeled with endocytosed HPTS in vivo were incubated for 20 min at 37°C in vitro, the acidic pH was

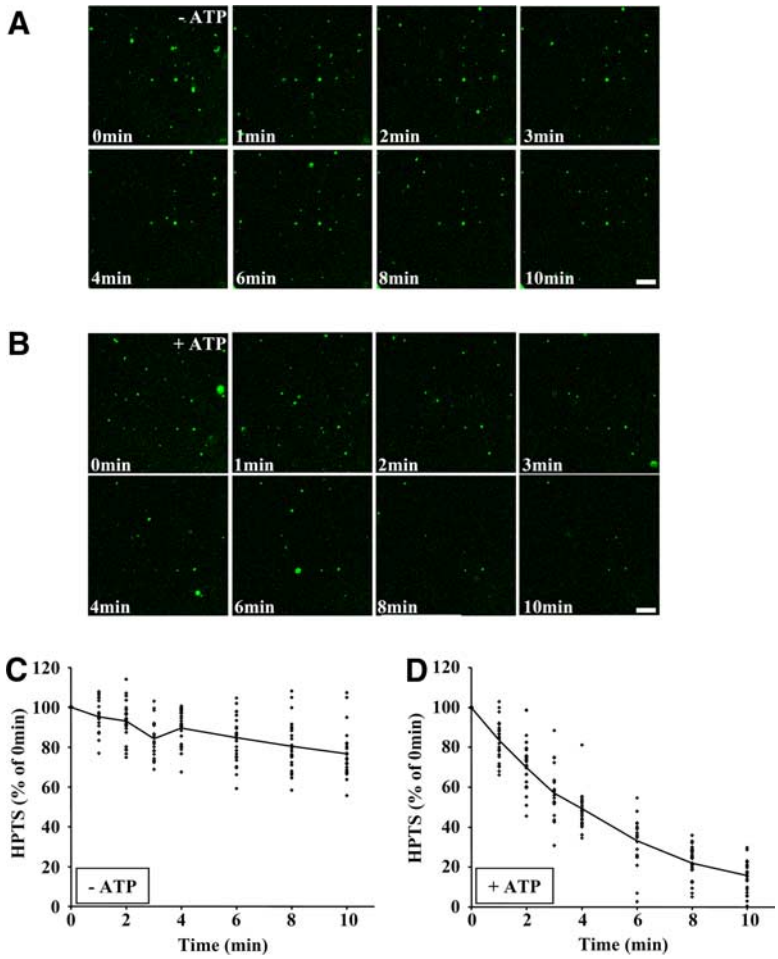

Figure 4. In vitro assay measuring HPTS release via back-fusion. (A and B) The in vitro assay was performed with protocol 1 (Figure 1A) to load newly formed lumenal vesicles with HPTS. After fractionation, late endosomes, which had been preloaded with HPTS, were reincubated using protocol 2 but without HPTS, in the absence (A) or presence (B) of ATP. The process was followed by videomicroscopy for 10 min at 37°C and frames were captured at the indicated times. Bars, 20 μm. (C and D) HPTS fluorescence was quantified at each time point in the experiments shown in A and B in the absence (C) or presence (D) of ATP, for 25 structures from three independent experiments. Values are expressed as a percentage of the fluorescence measured at t = 0 min, with the solid line showing the average.

maintained in a process sensitive to the V-ATPase inhibitor bafilomycin A1 or to ATP depletion (Figure 5C), as expected (Mellman *et al.*, 1986). Moreover, we found that HPTS incorporation was inhibited by bafilomycin A1, demonstrating that an active V-ATPase was necessary to support the budding process in vitro (Figure 5D). HPTS incorporation was also inhibited by the ionophore nigericin, which neutralizes the pH without altering the net positive charge, indicating that the acidogenic, but not the electrogenic, properties of the V-ATPase were required for lumenal vesicle formation (Figure 5D). These findings agree well with our previous observations that liposomes containing the late endosomal lipid lysobisphosphatidic acid (LBPA) spontaneously became multivesicular when their lumen was acidic (Matsuo *et al.*, 2004). We conclude that endosome acidification is required for the biogenesis of intralumenal vesicles.

Alix Regulates the Formation of Intralumenal Vesicles in Late Endosomes

Previous studies have demonstrated that depletion or mutagenesis of ESCRTs and Alix affect the dynamics of intraendosomal membranes (Hurley and Emr, 2006; Odorizzi, 2006; Slagsvold *et al.*, 2006; van der Goot and Gruenberg, 2006). However, it is not always easy to distinguish direct from indirect effects in these experiments, and the precise functions of these proteins are not known. Therefore, we applied our assay to first investigate the possible role of Alix in the formation of intralumenal vesicles. When the assay was carried out in the presence of increasing amounts of purified recombinant Alix (Figure 6A), the formation of intralumenal vesicles in late endosomes was inhibited in a dose-dependent manner (Figure 6B). By contrast, vesicle formation was not affected by excess recombinant Annexin A2 (Figure 6B), a protein necessary for early-to-late endosome transport but not for the formation of lumenal vesicles (Mayran *et al.*, 2003). Interestingly, we had previously observed that excess Alix inhibited the spontaneous pH-dependent formation of multivesicular liposomes containing LBPA in vitro (Matsuo *et al.*, 2004). Conversely, multivesicular liposome formation was stimulated by Alix-depleted cytosol (Matsuo *et al.*, 2004). In agreement with these observations, the formation of intralumenal vesicles within late endosomes in vitro was strongly stimulated when using PNS from cells that have been depleted of Alix with siRNAs (Figure 6D), even though depletion was not complete (Figure 6C; ≈90% after quantification of the blots). Under these conditions, late endosome recovery in gradients was not affected to any significant extent (Figure 6E). Strikingly, when early endosomes were recovered and analyzed in parallel experiments, we found that excess Alix did not interfere with the formation of HPTS-containing intralumenal vesicles in early endosomes (Figure 6B), whereas the process was only marginally affected by Alix depletion with siRNAs (Supplemental Figure S6D). These observations thus suggest that Alix negatively regulates the formation of intralumenal vesicles within late endosomes, as it does within liposomes (Matsuo *et al.*, 2004),

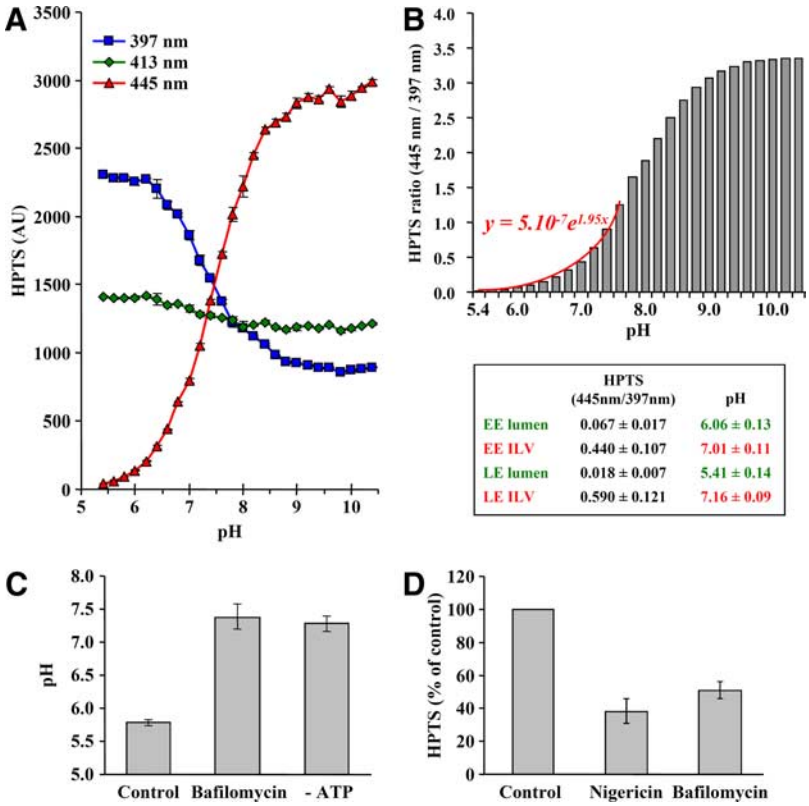

Figure 5. Characterization of lumenal vesicles. (A) The fluorescence emission at 510 nm of 2 μM HPTS was measured after excitation at the indicated wavelengths in 200 μl salt solution (150 mM NaCl) buffered between pH 5.4 and 10.4 with 20 mM MES (pH 5.4–6.6), HEPES (pH 6.8–8.2), and AMPSO (pH 8.4–10.4). Note that only 397- and 445-nm excitation wavelengths are pH-sensitive. (B) The ratio of HPTS fluorescence emission after excitation at 445 and 397 nm is represented as a function of pH. Results from pH 5.4–7.6 fit the indicated exponential equation. Note that error bars are too small to be seen. Inset, the endosomal pH (lumen) was measured after continuous HPTS endocytosis for 60 min at 37°C followed by subcellular fractionation to prepare early endosomes (EE) and late endosomes (LE). Alternatively, HPTS was incorporated into intralumenal vesicles (ILV) in vitro using protocol 1, and then EE and LE fractions were prepared (Figure 1A). The pH was calculated from the fluorescence ratio measured in each case after excitation at 445 and 397 nm. For each condition, means (± SEM) of at least five independent experiments are shown. (C) Late endosomes prepared from cells that had been incubated with HPTS for 60 min at 37°C in vivo were incubated in vitro using protocol 2 (but without HPTS) for 20 min at 37°C with or without bafilomycin A1 or ATP. Then the ratio of fluorescence after excitation at 445 and 397 nm were measured and pH calculated as in B. Means (± SEM) of three independent experiments are represented. (D) The in vitro assay was performed with protocol 1 (Figure 1A) in the presence of nigericin or bafilomycin A1, as indicated. HPTS fluorescence is expressed as a percentage of the untreated control. Means (± SEM) of three independent experiments are represented.

perhaps because the protein interacts with postfusion or prefission intermediates present on the limiting membrane.

Role of the ESCRT-I Subunit Tsg101 in Intralumenal Vesicle Formation

Previous studies have shown that Alix interacts with the ESCRT-I subunit Tsg101 in animal cells (Strack *et al.*, 2003; von Schwedler *et al.*, 2003), and consistently, Alix-GST interacted with endogenous Tsg101 present in rat liver cytosol (Supplemental Figure S6A). To get further insights into the molecular mechanisms regulating intralumenal vesicle formation, we thus investigated whether Tsg101 was also involved in the process. We were unable to obtain full-length recombinant Tsg101 using bacterial systems, as previously reported by others (Pornillos *et al.*, 2002) and thus decided to use an RNAi approach. Because the hamster genome is not fully sequenced, we analyzed the *tsg101* locus in BHK cells and designed three different siRNAs against BHK *tsg101*. All three knocked down Tsg101 expression, but to varying degrees (Supplemental Figure S6B). siRNA 2 efficiently depleted Tsg101, but also Hrs, possibly as a consequence of destabilizing the Hrs-ESCRT machinery, whereas siRNA 3 was somewhat less efficient than siRNA 1 (Supplemental Figure S6B). We thus preferred siRNA 1 (Figure 6C and Supplemental Figure S6C) so that significant Tsg101 knockdown was achieved, without affecting levels of Hrs (Supplemental Figure S6B), Alix or the other endosomal markers that were tested (Figure 6C). However, the effects of siRNA 1 could all be reproduced using the other siRNAs, albeit to varying extent depending on knockdown efficiency.

Knockdown of Tsg101 with siRNA 1 strongly reduced the intralumenal budding of HPTS-containing vesicles (Figure 6D), without affecting late endosome recovery in our gradients to any significant extent (Figure 6E). Strikingly, the effects of Tsg101 knockdown were opposite to those observed after Alix depletion in parallel experiments (Figure 6D). When both proteins were simultaneously depleted (Figure 6C), endosome recovery on gradients was unaffected (Figure 6E), and intralumenal vesicle formation was reduced when compared with the mock-treated control (Figure 6D). However, this effect was less severe than after knockdown of Tsg101 alone, as if the process recovered somewhat by concomitant Alix depletion. The effects of Alix or Tsg101 knockdown were not due to gross changes in the endocytic pathway. Indeed, under all conditions that we tested (Figure 7A), HPTS was incorporated into late endosomes containing BSA-Cy3 that had been endocytosed in vivo for 10 min at 37°C followed by a 40-min chase without the marker (Figure 7B). Quantification of these data showed that more than 80% of the vesicles containing HPTS were BSA-Cy3–positive after knockdown of Alix, Tsg101, or both (Figure 7C).

Next, we prepared late endosomes (Figure 8A) and cytosols (Figure 8B) separately from cells that had been treated with Tsg101 siRNA 1 or mock-treated, and we tested their capacity to support intralumenal vesicle formation in vitro. As expected (Figure 6D), the process was inhibited when depleted endosome and depleted cytosol were mixed (Figure 8C). However, mock-treated cytosol could rescue intralumenal vesicle formation within Tsg101-depleted late endosomes, and conversely mock-treated endosomes supported intralumenal budding in the presence of depleted cytosol (Figure 8C). These observations fully support the notion that ESCRTs cycle between membrane and cytosol (Hurley and Emr, 2006; Nickerson *et al.*, 2007; Williams and Urbe, 2007). But, they also indicate that Tsg101 siRNAs are unlikely to cause indirect or toxic effects, because both cytosol and endosome retain the competence to support in vitro budding after depletion, provided that they are incu-

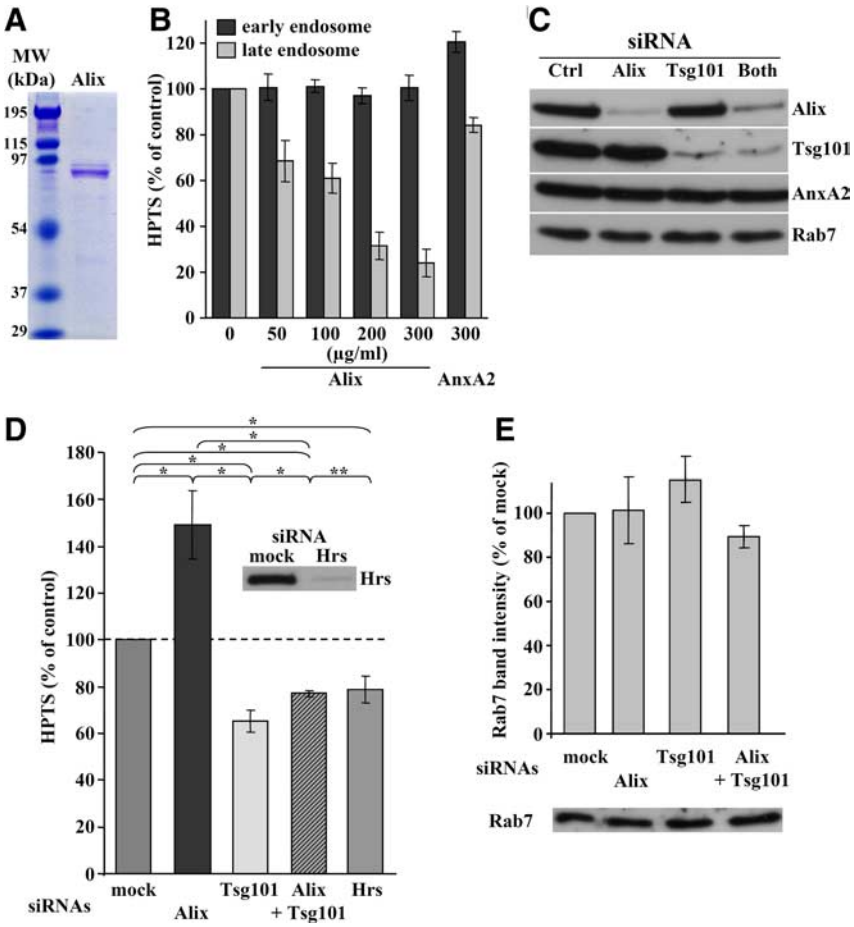

Figure 6. Effects of Alix and Tsg101 down-expression on budding in vitro. (A) The purified recombinant Alix was analyzed by SDS-PAGE, and the gel was stained with Coomassie blue. The left lane shows the indicated MW markers. (B) Recombinant Alix or Annexin A2 (AnxA2) was added at the indicated concentrations during the in vitro assay with protocol 1 (Figure 1A). After DPX quenching and cell fractionation, remaining HPTS fluorescence associated with early and late endosome fractions was measured and is expressed as a percentage of the controls. Means (± SEM) of three independent experiments are shown. (C) After treatment with control siRNA, siRNAs against Alix, Tsg101, or both, PNSs were prepared and analyzed by immunoblotting, as indicated. (D) The in vitro assay with protocol 1 (Figure 1A) was performed after knockdown of the indicated proteins with siRNAs. Means (± SEM) of HPTS fluorescence associated with late endosome fractions from at least five independent experiments per condition are represented. The chi-square test shows that each value is significantly different from the others (* $p < 0.01$), except when indicated (** $p > 0.01$). Inset, Hrs knockdown analyzed by Western blotting. (E) Cells were treated with siRNAs as in C and D. Late endosomes were prepared and analyzed by Western blotting with antibodies against Rab7. Western blots were quantified and means (± SEM) of three independent experiments are shown as percentages of the mock-treated controls.

bated with nondepleted endosomes or cytosol as a source of Tsg101.

Hrs knockdown (Figure 6D, inset) had little, if any, effect on intralumenal vesicle formation in late (Figure 6D) or early (Supplemental Figure S6D) endosomes, but it is not clear whether Hrs is directly involved in the formation of intralumenal vesicles (Gruenberg and Stenmark, 2004; Pons *et al.*, 2008). We then used the dominant negative mutant K173Q of the triple A ATPase Vps4 (Morita *et al.*, 2007a), which releases ESCRT-III from membranes (Hurley and Emr, 2006), to further investigate the role of ESCRTs in our assay. Upon overexpression, the GFP-tagged version of WT human Vps4 was predominantly cytosolic (Supplemental Figure S7A). By contrast, the mutant exhibited a characteristic punctate pattern (Supplemental Figure S7A) reflecting impaired endosomal functions (Williams and Urbe, 2007), although both proteins were expressed to similar levels (Supplemental Figure S7B; note that the antibody against human Vps4 does not cross-react with hamster). In our assay, the formation of intralumenal vesicles was inhibited by Vps4K173Q, but not by WT Vps4 (Figure 8D; Vps4K173Q effects are likely to be underestimated because the transfection rate of BHK cells is ≈50%). These observations further demonstrate that ESCRTs control the formation of intralumenal vesicles in our assay.

Electron Microscopy Analysis after Tsg101 or Alix Knockdown

Having shown that Alix and Tsg101 regulated HPTS incorporation in vitro, we used nanogold to investigate the effects of Alix and Tsg101 depletion by electron microscopy. When the in vitro assay was carried out at 4°C, only a few gold particles were present in endosomes and remained on their outer periphery (Figure 9A). By contrast, nanogold particles were found inside multivesicular endosomes after incubation for 20 min at 37°C in vitro (Figure 9B, with quantification in Figure 9G), as expected (Figure 3B). Because amounts of nanogold were limiting for quantification, gold enhancement was performed for longer times, resulting in a more heterogeneous distribution of particle sizes (Figure 9, A–F). Tsg101 or Alix depletion did not seem to affect the size of endosomes to any significant extent (Supplemental Figure S8), in agreement with previous observations after Tsg101 (Razi and Futter, 2006) or Alix (Matsuo *et al.*, 2004) knockdown. After partial Alix knockdown (Figure 6C), endosome morphology did not appear to be significantly affected (Figure 9C). Similarly, under our conditions of Tsg101 knockdown, some profiles appeared similar to controls (Figure 9D), and others contained fewer vesicles (Figure 9E), presumably because different endosome regions are differentially sensitive to Tsg101 depletion. A similar heterogeneity, including within the same cell, was observed by others (Razi and Futter, 2006). In any case, Tsg101 depletion caused a significant decrease in the number of gold particles per profile (Figure 9, D and E), whereas this number increased after Alix depletion (Figure 9C), without affecting the number of gold particles associated to the limiting membrane (quantification in Figure 9G). Strikingly, the number of gold particle per profile after knockdown of both Tsg101 and Alix was very similar to controls (Figure 9F, with quantification

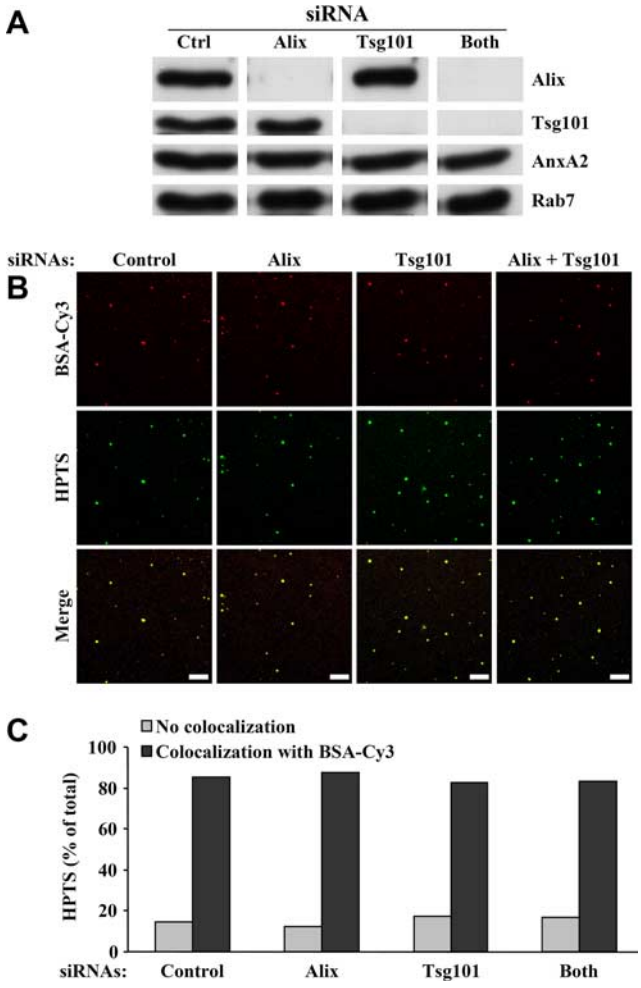

Figure 7. HPTS is incorporated into late endosomes after Alix and Tsg101 knockdown. BHK cells that had been treated for 3 d with the indicated siRNAs were incubated with BSA-Cy3 for 10 min at 37°C and then for 40 min without the tracer, to label late endosomes. PNSs were prepared, and aliquots were analyzed by Western blotting with antibodies against the indicated proteins (A). The remaining PNSs were used to perform the in vitro assay with protocol 1 (Figure 1A), and, after fractionation, late endosomes were analyzed by confocal microscopy (B) as in Figures 2B and Supplemental Figure S2. Bars, 20 μm. Individual vesicles containing HPTS and BSA-Cy3 were counted and the percentage of HPTS-labeled vesicles that also contained BSA-Cy3 is expressed as a percentage of the total number of HPTS-positive vesicles in each experiment (C). We analyzed 195 (control siRNAs), 196 (Alix siRNAs), 238 (Tsg101 siRNAs), and 265 (Both siRNAs) individual HPTS-positive structures from three independent experiments.

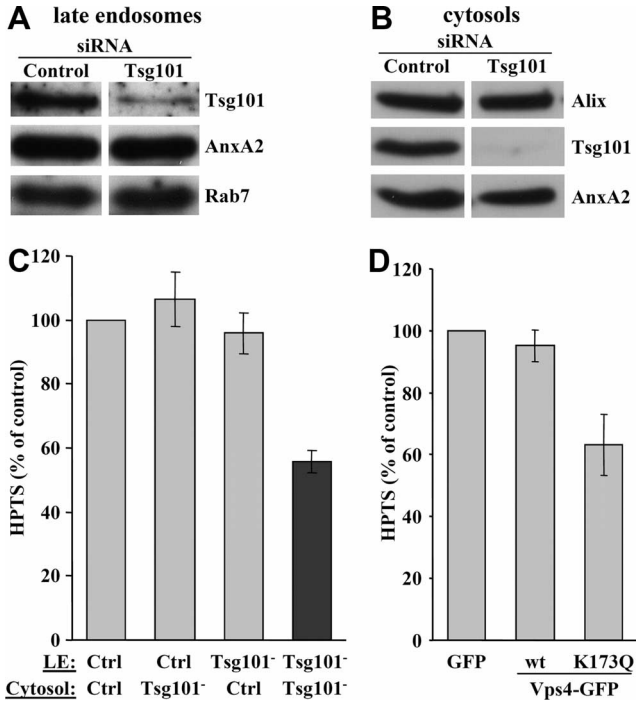

Figure 8. Tsg101 and hVps4. (A and B) BHK cells were mock-treated (control) or treated with siRNAs against Tsg101. Late endosomal fractions (A) and cytosols (B) were prepared separately and analyzed by Western blot using the indicated antibodies. (C) The in vitro budding assay was performed with protocol 2 (Figure 1A) using the late endosomes (LE) and cytosols prepared from mock-treated cells (control) and cells treated with Tsg101 siRNA (Tsg101^{--}) in A and B. The values are expressed as a percentage of the mock-treated control. Means (± SEM) of three independent experiments are represented. (D) GFP, WT Vps4-GFP, or Vps4K173Q-GFP was expressed in BHK cells (Supplemental Figure S7), and PNSs were prepared from each cell population. The in vitro assay was performed using these PNSs with protocol 1 (Figure 1A). Values are expressed as a percentage of the control with GFP alone. It should be noted that the transfection rate of BHK cells is ≈50% and thus that the effect of Vps4K173Q may well be underestimated. Means (± SEM) of four independent experiments are represented.

in Figure 9G). These data thus confirm our biochemical analysis after HPTS incorporation (Figure 6D) that Alix and Tsg101 control the formation of intralumenal vesicles, but act in an antagonistic manner.

EGF Receptor Sorting into Intralumenal Vesicles in Vitro

Because intralumenal vesicle formation could be reconstituted in vitro, we investigated whether we could measure EGF receptor sorting into intralumenal vesicles. To this end, we used our BHK cells that express GFP-tagged EGF receptor under the control of a tetracycline promoter (Figure 3, D–F), because these cells are optimal for subcellular fractionation (Petiot *et al.*, 2003). Indeed, the EGF receptor increased with time in late endosomal fractions prepared from cells that had been stimulated with EGF for increasing time periods (Figure 10A). Late endosomes fractions containing EGF receptor endocytosed for 30 min at 37°C were treated with TPCK-treated trypsin to shave the cytoplasmic face of the endosome limiting membrane. After trypsin inhibition with the soybean trypsin inhibitor, membranes were analyzed by gel electrophoresis and Western blotting. Under control conditions, ~50% of the EGF receptor became resistant to trypsin during the in vitro incubation (Figure 10D), as assessed with antibodies against the cytoplasmically exposed GFP. By contrast, EGF receptor was fully digested in the presence of detergent (data not shown). This incorporation of EGF receptor into trypsin-resistant membranes was specific, because the small GTPase Rab7, which is present on the limiting membrane of late endosomes (Zerial and McBride, 2001), was completely digested by trypsin, whereas a lumenal epitope of the type I transmembrane glycoprotein Lamp1 remained trypsin-insensitive (Aniento *et al.*, 1993a; Figure 10C). When the same experiment was repeated after Alix depletion (Figure 10B), EGF receptor protection against trypsin was significantly increased, whereas Rab7 remained fully trypsin-sensitive (Fig-

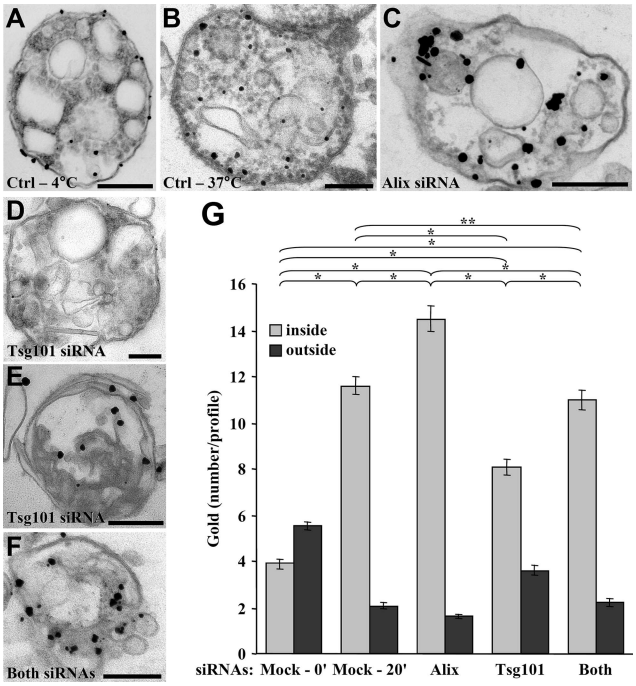

Figure 9. Ultrastructural analysis after Alix and Tsg101 knockdown. (A–F) Cells were first treated with control siRNAs (A and B) or siRNAs against Alix (C), Tsg101 (D and E), or both (F), as in Figure 6, C–E. Then, PNSs were prepared, used in the in vitro assay for 0 min (A) or 20 min (B–F) at 37°C in the presence of nanogold (Figure 1A, protocol 1), and processed for electron microscopy as in Figure 3, A and B. (A and F) Representatives of three independent experiments. Bars, 200 nm. (G) The number of nanogold particles per profile in A–F was quantified. The chi-square test shows that the values for single knockdowns are significantly different (* $p < 0.01$), whereas the double Alix-Tsg101 knockdown is not significantly different from the positive control at 20 min (** $p > 0.01$). Means (± SEM) of three independent experiments are shown.

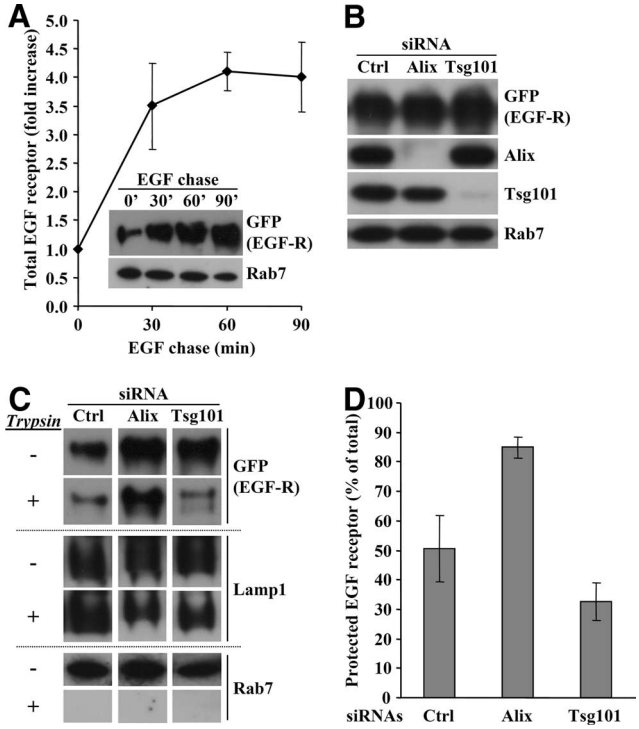

Figure 10. Sorting of EGF receptor into late endosomes. (A) BHK cells expressing the GFP-tagged human EGF receptor under the control of a tetracycline promoter were treated with 1 μg/ml doxycycline 24 h before the experiment. Cells were serum-starved for 1 h at 37°C in the presence of 10 μg/ml cycloheximide (which remained present throughout the experiment) and incubated with 200 ng/ml EGF for 1 h on ice and then for the indicated time periods (chase) at 37°C. Late endosome fractions were prepared and analyzed by Western blotting using antibodies against GFP or Rab7 (inset). Blots were quantified and the increase in EGF receptor appearance in late endosomes was normalized to the amounts detected at t = 0 min and expressed as fold increase. The means (± SEM) of three independent experiments are shown. (B) BHK cells expressing EGF receptor-GFP as in A were treated for 3 d with siRNAs against Alix or Tsg101. As in A, cells were treated with EGF for 30 min at 37°C, and PNSs were analyzed by Western blotting using the indicated antibodies. (C and D) Late endosome fractions were prepared from the PNSs in B. Each fraction was divided into two aliquots that were or not treated with trypsin for 15 min at 37°C. After blocking trypsin with soybean trypsin inhibitor, samples were analyzed by Western blotting using the indicated antibodies (C). The blots were scanned and the signals quantified. For each condition, the amounts of EGF receptor that was protected against trypsin are expressed as a percentage of the total receptor present in the control without trypsin (D). The means (± SEM) of three independent experiments are shown.

ure 10, C and D). By contrast, the receptor became more sensitive to trypsin after Tsg101 knockdown (Figure 10B), whereas Lamp1 remained unaffected (Figure 10, C and D). These data demonstrate that the EGF receptor was incorporated into lumenal vesicles that were formed within late endosomes in vitro. Moreover, they also demonstrate that EGF receptor sorting into intralumenal membranes is controlled by the opposite action of Alix and Tsg101, much like HPTS incorporation.

DISCUSSION

In this study, we describe a novel biochemical assay that reconstitutes the budding of membrane invaginations toward the lumen of endosomes, leading to the formation of intralumenal vesicles. The process is quantified by measuring the incorporation of the fluorescent solute HPTS within newly formed vesicles that budded into the endosome lumen. These data indicate that intralumenal vesicles may represent ≈10% of the total volume of late endosomes in BHK cells (Griffiths *et al.*, 1989), a value that fits nicely with electron microscopy observations by others (Futter *et al.*, 2001; Murk *et al.*, 2003; Mari *et al.*, 2008) and us (Le Blanc *et al.*, 2005). Indeed, a multivesicular endosome of 0.4–0.5-μm diameter contains ≈30–60 vesicles (50–60-nm diameter), representing in total ≈8–15% of the organelle volume. We find that uptake of HPTS within endosomes occurs relatively rapidly and then levels off with an apparent $t_{1/2} \approx 7.5$ min. In a concomitant process, however, preformed lumenal vesicles undergo fusion with the endosome membrane with similar kinetics, thereby releasing preloaded HPTS into the medium. This is supported by previous observations that lumenal vesicles can undergo back-fusion with the late endosome limiting membrane (van der Goot and Gruenberg, 2006), a process hijacked by the anthrax toxin (Abrami *et al.*, 2004) and vesicular stomatitis virus (Le Blanc *et al.*, 2005). Lumenal vesicles thus seem to undergo permanent cycles of fission and fusion at the limiting membrane, suggesting that they form a highly dynamic membrane network within the late endosome lumen.

The consensus view is that lumenal vesicles, once formed during the biogenesis of MVBs on the early endosome membrane, are targeted to lysosomes and degraded together with their cargo of signaling receptors (Gruenberg and Stenmark, 2004; Piper and Katzmann, 2007). It has been suggested that the activated EGF receptor is trafficked through a subpopulation of multivesicular endosomes in a process that involves annexin A1 (White *et al.*, 2006). However, we find that all endosomes that incorporated nanogold into newly formed lumenal vesicles in vitro also contained endocytosed EGF receptor and, conversely, that the EGF receptor is itself sorted into lumenal vesicles in a process controlled by the opposite actions of Alix and Tsg101, like HPTS incorporation. An alternative explanation comes from the observations that multivesicular endosomes contain more than one type of lumenal vesicles (Gillooly *et al.*, 2000; Kobayashi *et al.*, 2002; Sobo *et al.*, 2007a), raising the possibility that some are involved in the transport of signaling receptors to the lysosomes, whereas others undergo fusion at the limiting membrane. If so, intralumenal mechanisms must control the fate of intralumenal vesicles, back-fusion or degradation, including perhaps LBPA via its effector Alix, because Alix knockdown inhibits back-fusion (Abrami *et al.*, 2004; Le Blanc *et al.*, 2005) but not EGF receptor degradation (Schmidt *et al.*, 2004; Cabezas *et al.*, 2005). In addition, it cannot be excluded that some signaling receptors are returned to the endosome-limiting membrane via back-fusion and then recaptured within newly formed vesicles, perhaps like the EGF receptor in our assay, a mechanism that may contribute to explain MAPK signaling from late endosomes (Teis *et al.*, 2002; Taub *et al.*, 2007). Lumenal vesicles may also exchange membrane constituents and mix their contents via direct lumenal fusion events. Either fission and fusion cycle, with the limiting membrane or among lumenal vesicles, may account for our observations that both endocytosed EGF receptor and nanogold could be observed within the same lumenal vesicles.

Although there is no doubt that Hrs and ESCRTs regulate sorting of ubiquitinated receptors into lumenal vesicles, the mechanism that concentrates receptors at the site of vesicle formation is not clear, involving perhaps a conveyor belt-like (Hurley and Emr, 2006) or concentric (Nickerson *et al.*, 2007) subunit organization. Neither is it clear what controls the membrane deformation and budding processes (Williams and Urbe, 2007; Hanson *et al.*, 2008). We previously found that the formation of multivesicular liposomes in a protein-free system requires the late endosome lipid LBPA (Matsuo *et al.*, 2004) and a low lumenal pH, perhaps because LBPA can induce bilayer asymmetry and thus invagination (Matsuo *et al.*, 2004). In our assay, anti-LBPA antibodies did not have much effect, possibly because LBPA is masked by proteins on the cytosolic face of the membrane (P.-P. Luyet, unpublished data). However, the notion that membrane lipids are involved is supported by our observations that cholesterol accumulation, which alters membrane biophysical properties and reduces bilayer fluidity, inhibits the formation of lumenal vesicles. Moreover, our previous studies show that excess Alix inhibits the formation of multivesicular liposomes (Matsuo *et al.*, 2004). Similarly, we now find that excess Alix also inhibits the formation of intraendosomal vesicles, whereas the process is accelerated by Alix depletion, perhaps because Alix contributes to retain postfusion or prefission vesicular intermediates on the limiting membrane of late endosomes, during intralumenal cycles of fusion and fission. Consistently with this notion, Alix depletion also stimulates EGF receptor sorting into lumenal membranes.

Alix interacts with the ESCRT-I subunit Tsg101 during retrovirus budding at the plasma membrane (Strack *et al.*, 2003; von Schwedler *et al.*, 2003; Munshi *et al.*, 2006; Fisher *et al.*, 2007; Gottlinger, 2007) and cytokinesis (Carlton and Martin-Serrano, 2007; Morita *et al.*, 2007b). Similarly, we find that both proteins not only interact with each other, but also act together in the lumenal budding process. Our data demonstrate that Tsg101 is required for the formation of intralumenal vesicles in late endosomes, which is consistent with the fact that the bulk of the protein is present on this compartment at steady state (Bache *et al.*, 2003a). In contrast, we find that Hrs is not involved in the process. However, the functions of Hrs in lumenal vesicle formation (Lloyd *et al.*, 2002; Bache *et al.*, 2003b; Razi and Futter, 2006) are not clear and may well be indirect (Pons *et al.*, 2008). Although Alix negatively regulates the formation of lumenal vesicles and EGF receptor sorting, our data show that Tsg101 is a necessary component of the budding reaction. Hence, both proteins appear to act in an opposite but coordinated manner to control and tune the vesicle formation process. It is tempting to speculate that, once back-fusion has occurred, Alix is recruited onto the membrane and thereby traps potential postfusion or prefission intermediates. Then, in turn, Alix may recruit Tsg101 presumably together with its ESCRT partners, and trigger the membrane budding process. Alternatively, the proteins may act concomitantly, their selective inhibitory or stimulating effects then depending on mass-action law.

In conclusion, our study shows that intraendosomal vesicles form within late endosomes upon membrane budding toward the endosome lumen, and that this process is controlled by the regulatory functions of both Alix and Tsg101. Further investigations will be necessary to determine whether different populations of lumenal vesicles coexist within endosomes and what are their functions and to characterize the precise roles of Alix and ESCRTs in intraendosomal membrane dynamics.

ACKNOWLEDGMENTS

We thank Rémy Sadoul (Grenoble Institute of Neuroscience, Grenoble, France) and Harald Stenmark (The Norwegian Radium Hospital, Oslo, Norway) for the kind gifts of the pGex-6P2-Alix-GST construct and the anti-Hrs polyclonal antibody, respectively, as well as Wesley Sundquist (University of Utah School of Medicine, Salt Lake City, UT) for WT GFP-Vps4 and GFP-Vps4K173Q and Stefan Matile for help with pH calibration. We are grateful to Zeina Chamoun, Etienne Morel, Thierry Soldati, and Gisou van der Goot for critical reading of the manuscript, and members of our laboratory for helpful discussion. We also thank Marie-Hélène Beuchat and Brigitte Bernadets for their technical expertise. T.F. was a recipient of fellowships from the Fondation pour la Recherche Médicale and the Marie Curie IntraEuropean Programme within the 6th European Community Framework, and C.C.S. of a fellowship from the Human Frontier Science Program Organization. Support to J.G. was from the Swiss National Science Foundation and the Roche Foundation.

REFERENCES

Abrami, L., Lindsay, M., Parton, R. G., Leppla, S. H., and van der Goot, F. G. (2004). Membrane insertion of anthrax protective antigen and cytoplasmic delivery of lethal factor occur at different stages of the endocytic pathway. J. Cell Biol. *166*, 645–651.

Aniento, F., Emans, N., Griffiths, G., and Gruenberg, J. (1993a). Cytoplasmic dynein-dependent vesicular transport from early to late endosomes. J. Cell Biol. *123*, 1373–1387.

Aniento, F., Roche, E., Cuervo, A. M., and Knecht, E. (1993b). Uptake and degradation of glyceraldehyde-3-phosphate dehydrogenase by rat liver lysosomes. J. Biol. Chem. *268*, 10463–10470.

Babst, M. (2005). A protein's final ESCRT. Traffic *6*, 2–9.

Bache, K. G., Brech, A., Mehlum, A., and Stenmark, H. (2003a). Hrs regulates multivesicular body formation via ESCRT recruitment to endosomes. J. Cell Biol. *162*, 435–442.

Bache, K. G., Raiborg, C., Mehlum, A., and Stenmark, H. (2003b). STAM and Hrs are subunits of a multivalent ubiquitin-binding complex on early endosomes. J. Biol. Chem. *278*, 12513–12521.

Bradford, M. M. (1976). A rapid and sensitive method for the quantitation of microgram quantities of protein utilizing the principle of protein-dye binding. Anal. Biochem. *72*, 248–254.

Burnette, W. N. (1981). "Western blotting": electrophoretic transfer of proteins from sodium dodecyl sulfate-polyacrylamide gels to unmodified nitrocellulose and radiographic detection with antibody and radioiodinated protein A. Anal. Biochem. *112*, 195–203.

Cabezas, A., Bache, K. G., Brech, A., and Stenmark, H. (2005). Alix regulates cortical actin and the spatial distribution of endosomes. J. Cell Sci. *118*, 2625–2635.

Carlton, J. G., and Martin-Serrano, J. (2007). Parallels between cytokinesis and retroviral budding: a role for the ESCRT machinery. Science *316*, 1908–1912.

Cavalli, V., Vilbois, F., Corti, M., Marcote, M. J., Tamura, K., Karin, M., Arkinstall, S., and Gruenberg, J. (2001). The stress-induced MAP kinase p38 regulates endocytic trafficking via the GDI:Rab5 complex. Mol. Cell *7*, 421–432.

Chatellard-Causse, C., Blot, B., Cristina, N., Torch, S., Missotten, M., and Sadoul, R. (2002). Alix (ALG-2-interacting protein X), a protein involved in apoptosis, binds to endophilins and induces cytoplasmic vacuolization. J. Biol. Chem. *277*, 29108–29115.

Chevallier, J., Chamoun, Z., Jiang, G., Prestwich, G., Sakai, N., Matile, S., Parton, R. G., and Gruenberg, J. (2008). Lysobisphosphatidic acid controls endosomal cholesterol levels. J. Biol. Chem. (*in press*).

Doyotte, A., Russell, M. R., Hopkins, C. R., and Woodman, P. G. (2005). Depletion of TSG101 forms a mammalian "Class E" compartment: a multicisternal early endosome with multiple sorting defects. J. Cell Sci. *118*, 3003–3017.

Fernandez-Borja, M., Wubbolts, R., Calafat, J., Janssen, H., Divecha, N., Dusseljee, S., and Neefjes, J. (1999). Multivesicular body morphogenesis requires phosphatidyl-inositol 3-kinase activity. Curr. Biol. *9*, 55–58.

Fisher, R. D., Chung, H. Y., Zhai, Q., Robinson, H., Sundquist, W. I., and Hill, C. P. (2007). Structural and biochemical studies of ALIX/AIP1 and its role in retrovirus budding. Cell. *128*, 841–852.

Forgac, M. (2007). Vacuolar ATPases: rotary proton pumps in physiology and pathophysiology. Nat. Rev. Mol. Cell Biol. *8*, 917–929.

Frelin, C., Vigne, P., Ladoux, A., and Lazdunski, M. (1988). The regulation of the intracellular pH in cells from vertebrates. Eur. J. Biochem. *174*, 3–14.

Futter, C. E., Collinson, L. M., Backer, J. M., and Hopkins, C. R. (2001). Human VPS34 is required for internal vesicle formation within multivesicular endosomes. J. Cell Biol. *155*, 1251–1264.

Gillooly, D. J., Morrow, I. C., Lindsay, M., Gould, R., Bryant, N. J., Gaullier, J. M., Parton, R. G., and Stenmark, H. (2000). Localization of phosphatidylinositol 3-phosphate in yeast and mammalian cells. EMBO J. *19*, 4577–4588.

Gorvel, J. P., Chavrier, P., Zerial, M., and Gruenberg, J. (1991). rab5 controls early endosome fusion in vitro. Cell *64*, 915–925.

Gottlinger, H. G. (2007). How HIV-1 hijacks ALIX. Nat. Struct. Mol. Biol. *14*, 254–256.

Griffiths, G., Back, R., and Marsh, M. (1989). A quantitative analysis of the endocytic pathway in baby hamster kidney cells. J. Cell Biol. *109*, 2703–2720.

Gruenberg, J. (2001). The endocytic pathway: a mosaic of domains. Nat. Rev. Mol. Cell Biol. *2*, 721–730.

Gruenberg, J., Griffiths, G., and Howell, K. E. (1989). Characterization of the early endosome and putative endocytic carrier vesicles in vivo and with an assay of vesicle fusion in vitro. J. Cell Biol. *108*, 1301–1316.

Gruenberg, J., and Stenmark, H. (2004). The biogenesis of multivesicular endosomes. Nat. Rev. Mol. Cell Biol. *5*, 317–323.

Gu, F., Aniento, F., Parton, R. G., and Gruenberg, J. (1997). Functional dissection of COP-I subunits in the biogenesis of multivesicular endosomes. J. Cell Biol. *139*, 1183–1195.

Hanson, P. I., Roth, R., Lin, Y., and Heuser, J. E. (2008). Plasma membrane deformation by circular arrays of ESCRT-III protein filaments. J. Cell Biol. *180*, 389–402.

Harder, T., Kellner, R., Parton, R., and Gruenberg, J. (1997). Specific release of membrane bound annexin II and cortical cytoskeletal elements by sequestration of membrane cholesterol. Mol. Biol. Cell *8*, 533–545.

Hurley, J. H., and Emr, S. D. (2006). The ESCRT complexes: structure and mechanism of a membrane-trafficking network. Annu. Rev. Biophys. Biomol. Struct. *35*, 277–298.

Kobayashi, T., Beuchat, M. H., Chevallier, J., Makino, A., Mayran, N., Escola, J. M., Lebrand, C., Cosson, P., and Gruenberg, J. (2002). Separation and characterization of late endosomal membrane domains. J. Biol. Chem. *277*, 32157–32164.

Kobayashi, T., Beuchat, M. H., Lindsay, M., Frias, S., Palmiter, R. D., Sakuraba, H., Parton, R. G., and Gruenberg, J. (1999). Late endosomal membranes rich in lysobisphosphatidic acid regulate cholesterol transport. Nat. Cell Biol *1*, 113–118.

Kobayashi, T., Stang, E., Fang, K. S., de Moerloose, P., Parton, R. G., and Gruenberg, J. (1998). A lipid associated with the antiphospholipid syndrome regulates endosome structure and function. Nature *392*, 193–197.

Laemmli, U. K. (1970). Cleavage of structural proteins during the assembly of the head of bacteriophage T4. Nature *227*, 680–685.

Le Blanc, I. *et al*. (2005). Endosome-to-cytosol transport of viral nucleocapsids. Nat. Cell Biol. *7*, 653–664.

Lebrand, C., Corti, M., Goodson, H., Cosson, P., Cavalli, V., Mayran, N., Faure, J., and Gruenberg, J. (2002). Late endosome motility depends on lipids via the small GTPase Rab7. EMBO J. *21*, 1289–1300.

Liscum, L., and Faust, J. R. (1989). The intracellular transport of low density lipoprotein-derived cholesterol is inhibited in Chinese hamster ovary cells cultured with 3- beta-[2-(diethylamino)ethoxy]androst-5-en-17-one. J. Biol. Chem. *264*, 11796–11806.

Lloyd, T. E., Atkinson, R., Wu, M. N., Zhou, Y., Pennetta, G., and Bellen, H. J. (2002). Hrs regulates endosome membrane invagination and tyrosine kinase receptor signaling in *Drosophila*. Cell *108*, 261–269.

Mari, M., Bujny, M. V., Zeuschner, D., Geerts, W. J., Griffith, J., Petersen, C. M., Cullen, P. J., Klumperman, J., and Geuze, H. J. (2008). SNX1 defines an early endosomal recycling exit for sortilin and mannose 6-phosphate receptors. Traffic *9*, 380–393.

Matsuo, H. et al. (2004). Role of LBPA and Alix in multivesicular liposome formation and endosome organization. Science *303*, 531–534.

Maxfield, F. R., and McGraw, T. E. (2004). Endocytic recycling. Nat. Rev. Mol. Cell Biol. *5*, 121–132.

Maxfield, F. R., and Tabas, I. (2005). Role of cholesterol and lipid organization in disease. Nature *438*, 612–621.

Mayor, S., and Pagano, R. E. (2007). Pathways of clathrin-independent endocytosis. Nat. Rev. Mol. Cell Biol. *8*, 603–612.

Mayran, N., Parton, R. G., and Gruenberg, J. (2003). Annexin II regulates multivesicular endosome biogenesis in the degradation pathway of animal cells. EMBO J. *22*, 3242–3253.

Mellman, I., Fuchs, R., and Helenius, A. (1986). Acidification of the endocytic and exocytic pathways. Annu. Rev. Biochem. *55*, 663–700.

Morel, E., and Gruenberg, J. (2007). The p11/S100A10 light chain of annexin A2 is dispensable for annexin A2 association to endosomes and functions in endosomal transport. PLoS ONE *2*, e1118.

Morita, E., Sandrin, V., Alam, S. L., Eckert, D. M., Gygi, S. P., and Sundquist, W. I. (2007a). Identification of human MVB12 proteins as ESCRT-I subunits that function in HIV budding. Cell Host Microb. *2*, 41–53.

Morita, E., Sandrin, V., Chung, H. Y., Morham, S. G., Gygi, S. P., Rodesch, C. K., and Sundquist, W. I. (2007b). Human ESCRT and ALIX proteins interact with proteins of the midbody and function in cytokinesis. EMBO J. *26*, 4215–4227.

Munshi, U. M., Kim, J., Nagashima, K., Hurley, J. H., and Freed, E. O. (2006). An Alix fragment potently inhibits HIV-1 budding: characterization of binding to retroviral YPXL late domains. J. Biol. Chem. *282*, 3847–3855.

Murk, J. L., Humbel, B. M., Ziese, U., Griffith, J. M., Posthuma, G., Slot, J. W., Koster, A. J., Verkleij, A. J., Geuze, H. J., and Kleijmeer, M. J. (2003). Endosomal compartmentalization in three dimensions: implications for membrane fusion. Proc. Natl. Acad. Sci. USA *100*, 13332–13337.

Nickerson, D. P., Russell, M. R., and Odorizzi, G. (2007). A concentric circle model of multivesicular body cargo sorting. EMBO Rep. *8*, 644–650.

Odorizzi, G. (2006). The multiple personalities of Alix. J. Cell Sci. *119*, 3025–3032.

Parton, R. G., Schrotz, P., Bucci, C., and Gruenberg, J. (1992). Plasticity of early endosomes. J. Cell Sci. *103*, 335–348.

Petiot, A., Faure, J., Stenmark, H., and Gruenberg, J. (2003). PI3P signaling regulates receptor sorting but not transport in the endosomal pathway. J. Cell Biol. *162*, 971–979.

Piper, R. C., and Katzmann, D. J. (2007). Biogenesis and function of multivesicular bodies. Annu. Rev. Cell Dev. Biol. *23*, 519–547.

Pons, V., Luyet, P.-P., Morel, E., Abrami, L., van der Goot, F. G., Parton, R. G., and Gruenberg, J. (2008). Hrs and SNX3 functions in sorting and membrane invagination within multivesicular bodies. PLoS Biol. *6*, e214.

Pornillos, O., Alam, S. L., Rich, R. L., Myszka, D. G., Davis, D. R., and Sundquist, W. I. (2002). Structure and functional interactions of the Tsg101 UEV domain. EMBO J. *21*, 2397–2406.

Raiborg, C., Bremnes, B., Mehlum, A., Gillooly, D. J., D'Arrigo, A., Stang, E., and Stenmark, H. (2001). FYVE and coiled-coil domains determine the specific localisation of Hrs to early endosomes. J. Cell Sci. *114*, 2255–2263.

Raiborg, C., Wesche, J., Malerod, L., and Stenmark, H. (2006). Flat clathrin coats on endosomes mediate degradative protein sorting by scaffolding Hrs in dynamic microdomains. J. Cell Sci. *119*, 2414–2424.

Raymond, C. K., Howald-Stevenson, I., Vater, C. A., and Stevens, T. H. (1992). Morphological classification of the yeast vacuolar protein sorting mutants: evidence for a prevacuolar compartment in class E vps mutants. Mol. Biol. Cell *3*, 1389–1402.

Razi, M., and Futter, C. E. (2006). Distinct roles for Tsg101 and Hrs in multivesicular body formation and inward vesiculation. Mol. Biol. Cell *17*, 3469–3483.

Reaves, B. J., Bright, N. A., Mullock, B. M., and Luzio, J. P. (1996). The effect of wortmannin on the localisation of lysosomal type I integral membrane glycoproteins suggests a role for phosphoinositide 3-kinase activity in regulating membrane traffic late in the endocytic pathway. J. Cell Sci. *109*, 749–762.

Rojo, M., Peppercok, R., Emery, G., Kellner, R., Stang, E., Parton, R. G., and Gruenberg, J. (1997). Involvement of the transmembrane protein p23 in biosynthetic protein transport. J. Cell Biol. *139*, 1119–1135.

Schmidt, M. H., Hoeller, D., Yu, J., Furnari, F. B., Cavenee, W. K., Dikic, I., and Bogler, O. (2004). Alix/AIP1 antagonizes epidermal growth factor receptor downregulation by the Cbl-SETA/CIN85 complex. Mol. Cell. Biol. *24*, 8981–8993.

Simons, K., and Gruenberg, J. (2000). Jamming the endosomal system: lipid rafts and lysosomal storage diseases. Trends Cell Biol. *10*, 459–462.

Slagsvold, T., Pattni, K., Malerod, L., and Stenmark, H. (2006). Endosomal and non-endosomal functions of ESCRT proteins. Trends Cell Biol. *16*, 317–326.

Sobo, K., Chevallier, J., Parton, R. G., Gruenberg, J., and van der Goot, F. G. (2007a). Diversity of raft-like domains in late endosomes. PLoS ONE *2*, e391.

Sobo, K., Le Blanc, I., Luyet, P. P., Fivaz, M., Ferguson, C., Parton, R. G., Gruenberg, J., and van der Goot, F. G. (2007b). Late endosomal cholesterol accumulation leads to impaired intra-endosomal trafficking. PLoS ONE *2*, e851.

Strack, B., Calistri, A., Craig, S., Popova, E., and Gottlinger, H. G. (2003). AIP1/ALIX is a binding partner for HIV-1 p6 and EIAV p9 functioning in virus budding. Cell *114*, 689–699.

Sturley, S. L., Patterson, M. C., Balch, W., and Liscum, L. (2004). The pathophysiology and mechanisms of NP-C disease. Biochim. Biophys. Acta *1685*, 83–87.

Taub, N., Teis, D., Ebner, H. L., Hess, M. W., and Huber, L. A. (2007). Late endosomal traffic of the epidermal growth factor receptor ensures spatial and temporal fidelity of mitogen-activated protein kinase signaling. Mol. Biol. Cell *18*, 4698–4710.

Tedesco, M. M., and Matile, S. (1999). Spectroscopic detection of endovesiculation by large unilamellar phosphatidylcholine vesicles: effects of chlorpromazine, dibucaine, and safingol. Bioorg. Med. Chem. *7*, 1373–1379.

Teis, D., Wunderlich, W., and Huber, L. A. (2002). Localization of the MP1-MAPK scaffold complex to endosomes is mediated by p14 and required for signal transduction. Dev. Cell *3*, 803–814.

Urbe, S., Sachse, M., Row, P. E., Preisinger, C., Barr, F. A., Strous, G., Klumperman, J., and Clague, M. J. (2003). The UIM domain of Hrs couples receptor sorting to vesicle formation. J. Cell Sci. *116*, 4169–4179.

van der Goot, F. G., and Gruenberg, J. (2006). Intra-endosomal membrane traffic. Trends Cell Biol. *16*, 514–521.

von Schwedler, U. K. *et al.* (2003). The protein network of HIV budding. Cell *114*, 701–713.

White, I. J., Bailey, L. M., Aghakhani, M. R., Moss, S. E., and Futter, C. E. (2006). EGF stimulates annexin 1-dependent inward vesiculation in a multivesicular endosome subpopulation. EMBO J. *25*, 1–12.

Williams, R. L., and Urbe, S. (2007). The emerging shape of the ESCRT machinery. Nat. Rev. Mol. Cell Biol. *8*, 355–368.

Willoughby, D., Thomas, R. C., and Schwiening, C. J. (1998). Comparison of simultaneous pH measurements made with 8-hydroxypyrene-1,3,6-trisulphonic acid (HPTS) and pH-sensitive microelectrodes in snail neurones. Pfluegers Arch. *436*, 615–622.

Zerial, M., and McBride, H. (2001). Rab proteins as membrane organizers. Nat. Rev. Mol. Cell. Biol. *2*, 107–117.